理學博士學位論文

Neuronal regulation of peripheral organs mediated by calcium signaling

칼슘신호를 통한

말초 기관의 신경 조절 연구

2018년 8월

서울대학교 대학원

치의과학과 신경생물학 전공

김 윤 정

칼슘신호를 통한
말초 기관의 신경 조절 연구

지도교수 최 세 영

이 논문을 이학박사 학위논문으로 제출함

2018 년 5 월

서울대학교 대학원

치의과학과 신경생물학 전공

김 윤 정

김윤정의 이학박사 학위논문을 인준함

2018 년 7 월

위 원 장 　　　　　　　　　　 (인)

부위원장 　　　　　　　　　　 (인)

위　　원 　　　　　　　　　　 (인)

위　　원 　　　　　　　　　　 (인)

위　　원 　　　　　　　　　　 (인)

Neuronal regulation of peripheral organs mediated by calcium signaling

Advisor:
Prof. Se-Young Choi, Ph.D.

A dissertation submitted in partial fulfillment
of the requirements for the degree of
DOCTOR OF PHILOSOPHY

to the Faculty of
Program in Neuroscience
at
Department of Dental Science
The Graduate School of Seoul National University
by
Yoon-Jung Kim

Data Approved:
July, 2018

Seog Bae Oh

Se-Young Choi

Kyongpyo Park

Hee-Kyung Park

Mihye Lee

ABSTRACT

Neuronal regulation of peripheral organs mediated by calcium signaling

Yoon-Jung Kim

Program in Neuroscience
Department of Dental Science
The Graduate School of Seoul National University

Synapse is a fundamental structure in which two neurons communicate, and many studies have revealed the intercellular signaling of neurons. Understanding the structure and function of synapses is crucial to brain function research and the overcoming of synaptic disorders. Nerves play a role in controlling many organs in our body, including glands and muscles. Signal transduction between neurons and other cells around the synapse is very important not only in the central nervous system but also in the peripheral nervous system. Therefore, these studies are essential to understand the neural control of the organ in question at the molecular and cellular level.

One of peripheral system, salivary gland regulates their secretory functions through the neurotransmitter-generated Ca^{2+} signal. Increase of intracellular Ca^{2+} regulates ion channel activity in various domains in the cell and induces translocation of AQP5 channel to cause water secretion. These

salivary gland cells communicate with other cells mainly via G protein-coupled receptors (GPCRs). Therefore, understanding GPCRs in target organs, including exocrine glands, is crucial to understanding how receptive signals from neurons are accommodated.

First, I characterized the molecular mechanism of GPCR signaling in salivary gland. Recently, it has been shown that store-operated Ca^{2+} entry contributes significantly to GPCR-mediated Ca^{2+} entry. In this thesis, I investigated the characteristics of SOCE in human submandibular gland HSG cells with those of human embryonic kidney 293 (HEK293) cells, human leukemia T cell line Jurkat-T cells and human promyelocytoma HL-60. Results imply that, unlike most non-excitatory cells, SOCE in HSG cells is distinct from typical Orai-dependent SOCE.

I tried to identify a novel GPCR in salivary gland cells. I have characterized metabotropic Zn receptors on human submandibular gland cells. I found that ZnR/GPR39 is expressed in HSG cells. $ZnSO_4$ increased cytosolic Ca^{2+} concentration ($[Ca^{2+}]_i$). Both muscarinic antagonist and histaminergic antagonists did not have any effect on Zn-induced increases of $[Ca^{2+}]_i$. Zn-induced $[Ca^{2+}]_i$ completely blocked by PLC inhibitor and showed heterologous desensitization. These data suggest that metabotropic Zn receptors are involved in Ca^{2+} signaling in human submandibular gland cells, which is distinguished from other salivary gland G-protein-coupled receptors.

Next I studied a modulator of GPCR signaling in salivary gland cells. I have studied how chlorpromazine regulates intracellular calcium signaling in salivary glands. In the mouse model, chlorpromazine inhibited muscarinic-induced saliva secretion. Chlorpromazine inhibits muscarinic and histamine-induced $[Ca^{2+}]_i$ increases in HSG cells. Interestingly chlorpromazine inhibits both Ca^{2+} release from ER and Ca^{2+} influx via SOCE. These results suggest that chlorpromazine inhibits GPCR-mediated calcium signal through various

inhibitory sites such as ER and SOCE, thereby reducing salivation.

Finally, I focused on a modulator of the downstream pathway of GPCR-induced Ca^{2+} signaling in muscle cells. The BK channel, Ca^{2+} activated K channel is downstream of cytosolic Ca^{2+} signaling. Cereblon (CRBN) is a key factor that regulates the surface level of this BK channel, and binding with BK induces ER retention. I investigated whether a pathogenic R419X mutant form of CRBN rescues the phenotype observed in the CRBN KO mutant at the *Drosophila* NMJ. I observed that CRBN WT was expressed in the brain region, while CRBN R419X was expressed in the VNC and axonal terminal regions. Transfection of CRBN WT into CRBN KO cells in cultured hippocampal neurons also decreased BK channel activity, but transfection of CRBN R419X did not show a significant decrease in BK channel. These results suggest that the decrease of presynaptic release probability through BK channel increase can be induced by CRBN KO and point mutation (R419X).

These results suggest that Ca^{2+} signaling, as well as its upstream (i.e. GPCR) and downstream (i.e. Ca^{2+}-activated K^{+} channel) factors, is the critical modulator for the peripheral neurotransmission, and a core regulator target for the peripheral functions including exocrine glands and muscles.

Key words: Peripheral nervous system, Cytosolic Ca^{2+}, G-protein coupled receptors, Store-operated Ca^{2+} entry, Zinc, Chlorpromazine, BK channel

Student Number: 2007-22090

Contents

List of Figures

Chapter III.

Chapter IV.

Conclusion.

Abbreviation

AP	Action potential
AQP5	Aquaporin-5
CRBN	Cereblon
ER	Endoplasmic reticulum
GPCR	G-protein-coupled receptor
HSG	Human submandibular gland cells
HSY	Human salivary adenocarcinoma cells
Icrac	Ca^{2+} release activated Ca^{2+} current
ID	Intellectual disability
$I_{K(Ca)}$	Calcium-activated potassium currents
IP_3	Inositol 1,4,5-trisphosphate
PIP_2	Phosphatidylinositol 4,5 bisphosphate
PLC	Phospholipase C
PMCA	Plasma-membrane Ca^{2+}-ATPase
SERCA	Sarcoendoplasmic reticulum Ca^{2+}-ATPase
SOCE	Store-operated Ca^{2+} entry
TEVC	Two-electrode voltage-clamp
TG	Thapsigargin
TRPC	Transient Receptor Canonical
VOCE	Voltage-operated Ca^{2+} entry

General Introduction

Synapse is a fundamental structure in which two neurons communicate, and many studies have revealed the intercellular signaling of neurons. Understanding the structure and function of synapses is crucial to brain function research and the overcoming of synaptic disorders. Signaling in synapses plays a very important role in cognition, sensory perception, learning and memory, and decision-making. So far, many studies on synaptic plasticity have revealed the molecular and cellular mechanisms of brain function. These studies have addressed signal transduction between neurons in the central nervous system, mainly in the hippocampus and cerebral cortex. In order to precisely control synaptic signal transduction, it is necessary to control the synaptic structure and function through the interaction of the two cells forming the synapse. These interactions are mediated by cell adhesion molecules or secreted signal molecules (Siddiqui and Craig, 2011; Missler et al., 2012). It has been known that neuroligin and neurexin, which are typical cell adhesion molecules, play a key role in neurological function, and many studies have proved that these abnormalities cause various brain diseases called 'synaptopathy' such as autism or cognitive impairment (Rothwell et al., 2014; Anderson et al., 2015; Bemben et al., 2015).

The signaling of these synapses is not necessarily limited to the central nervous system. Nerves play a role in controlling many organs in our body, including glands and muscles. This regulation is mainly in the peripheral nerves, such as the autonomic nerves and the motor nerves, and their molecular identity is similar to the central nervous system. Therefore, signal transduction between neurons and other cells around the synapse is very important not only in the central nervous system but also in the peripheral

nervous system. Therefore, these studies are essential to understand the neural control of the organ in question at the molecular and cellular level.

Exocrine Gland as a target of peripheral nervous system.

The salivary gland is an exocrine gland formed by the epithelium surface inward, where saliva is formed and released into the oral cavity. The salivary gland consists of large salivary glands (submandibular glands, parotid glands, and sublingual glands) and minor salivary glands. The saliva secreted is mainly composed of electrolytes and water obtained from the blood plasma. Such saliva plays various roles such as providing moisture to the oral mucosa to keep it dry, thereby maintaining healthiness in the oral cavity, improving taste, lubricating action, buffering action and eliminating the occurrence of dental caries.

Exocrine cells, the salivary gland cells, regulate their secretion through the neurotransmitter-generated Ca^{2+} signal. Their saliva secretion is regulated by autonomic sympathetic and parasympathetic stimuli. Especially, acetylcholine secreted from parasympathetic nerve is known to be the most important salivary secretory factor in salivary glands. In order to enhance fluid secretion in the salivary gland, a series of processes is required: activation of the membrane receptor, production of the intracellular second messenger, migration of calcium, and stimulation of the ion transport pathway. When an increase in cytosolic Ca^{2+} ($[Ca^{2+}]_i$) occurs in the acinar cell where fluid secretion occurs, ion channel activity is regulated in various domains in the cell, and the water channel AQP5 channels are translocated to lumen and water secretion occurs . There are two steps, Ca^{2+} release from endoplasmic reticulum (ER, Ca^{2+} storage) and Ca^{2+} influx via plasma membrane, to increase $[Ca^{2+}]_i$ in the salivary gland and maintain the saliva secretion state

(Fig. 1).

[Ca^{2+}]$_i$ plays a very important role in regulating K^+, Na^+ and Cl^- flux in salivary acinar cells. Fluid secretion is maintained as long as [Ca^{2+}]$_i$ increases in acinar cell activates K^+ and Cl^- channels. For fluid secretion, transepithelial transport of Cl^- from the basolateral to apical side of the cell is required, and Na^+ flux through the tight junction accumulates NaCl in the lumen, resulting in water secretion through the AQP5 channel present in the apical membrane with the appropriate osmotic gradient. In addition, the apical and basolateral regions of the cell become a hyperpolarized state through K^+ efflux to support the fluid secretion. Cytosolic Ca^{2+} is maintained at about 50-100 nM in resting cells, which is smaller than the threshold that required to activate K^+ and Cl^- channels (Melvinetal, 2005; Ambudkar, 2014).

Ca^{2+} release from ER

G-protein mediated activation of phosphatidylinositol 4,5 bisphosphate (PIP$_2$)-specific phospholipase C (PLC) occurs when an external neurotransmitter binds to muscarinic, alpha-adrenergic, or purinergic receptors present in the plasma membrane and hydrolyzes PIP$_2$ into inositol 1,4,5-trisphosphate (IP$_3$). IP$_3$ binds to the IP$_3$ receptor (IP$_3$R) present in the ER membrane and releases Ca^{2+} in the ER through the receptor (Fig. 1). In exocrine gland cells, IP$_3$R2 and IP$_3$R3 are concentrated in the apical pole of the cell (Mikoshiba, 2008; Yule, 2010; Petersen, 2008), and intracellular calcium increases in the apical region when external stimuli are given. This increased intracellular calcium is spread to the basal pole (Melvin et al., 2005; Yule, 2001), which activates various ion channels and transporters to coordinate fluid secretion coordinately (Melvin et al., 2005; Ambudkar, 2012).

Ca^{2+} influx via plasma membrane

The intracellular calcium increase occurs not only in the Ca^{2+} release from the ER but also in the Ca^{2+} influx through channels at the plasma membrane. The latter is called store-operated Ca^{2+} entry (SOCE) and is caused by Ca^{2+} depletion of ER. STIM1 in the ER membrane acts as a Ca^{2+} sensor, which causes a conformational change when the ER calcium concentration is lowered and forms a Ca^{2+} entry channel with Orai or Transient Receptor Canonical (TRPC) present in the plasma membrane (Hogan et al., 2010; Yuan et al., 2009; Kee et al., 2010; Cheng et al., 2013). Orai1 is the most well characterized among the Orai channel family, which forms a highly Ca^{2+} - sensitive, inwardly rectifying Ca^{2+} current (Icrac) when activated by STIM1 (Hogan et al., 2010; Prakriya. 2009; Yuan et al., 2009). This channel functions as a Ca^{2+} permeable non-selective cation channel, and in particular all members are activated in response to PIP_2 hydrolysis stimulated by neurotransmitters (Birnbaumer et al., 1996; Montell, 2005). Perturbation of SOCE activity is thought to be an important toxic mechanism because SOCE keeps intracellular calcium pool constant and maintains GPCR signaling.

Intracellular Ca^{2+} signaling

Ca^{2+} was first recognized for its importance in physiological function by Sydney Ringer in the 1880s, and many studies have been found to be critical to various cell motility (gene transcription, muscle contraction) (Berridge et al., 2000; Rizzuto and Pozzan, 2006). Ca^{2+} modulates protein function by altering the shape and charge of binding proteins (similar to phosphorylation). In addition, its divalent cation is highly reactive and can bind strongly to water and precipitate phosphates compared to its cousin, Mg^{2+}. This

characteristic of calcium ions makes it necessary to control the concentration in cells, and uses compartments, extrusion or chelation to control calcium without chemical changes. Signal transduction is controlled through the affinity of hundreds of proteins that bind to calcium.

The compartment, the simplest method for intracellular concentration control, is due to the plasma membrane of the cell. The calcium signal in epithelia or cardiomyocyte is transmitted through connexon, a pathway through two cell membranes called gap junctions. However, in general, cell to cell signals are transmitted through channels such as nicotinic, purinergic (ionotropic), and NMDA receptors.

The intracellular calcium concentration is about 100 nM, whereas the extracellular calcium concentration is 2 mM, which is roughly 20,000 fold. Therefore, various toolkits are required to maintain calcium concentration in cytoplasm. There are ATPase pumps and exchangers to lower the cytoplasmic calcium concentration. The presence of PMCA in the plasma membrane of the cell and SERCA in the ER, the intracellular calcium reservoir, transport the cytoplasmic calcium into the extracellular or ER. In addition, Na^+, Ca^{2+} and K^+ are exchanged through NCKX and NCX present in the protoplasm. Conversely, when increased cytoplasmic calcium is required, various Ca^{2+} permeant channels and the PLC pathway through the GPCR are activated. Excitable cells such as neurons and muscle cells are activated by voltage-operated Ca^{2+} entry (VOCE), which is opened by depolarization, whereas nonexcitable cells such as salivary gland cells activate intracellular stores of the calcium-operated Ca^{2+} entry (SOCE) is activated.

G-protein coupled receptor signaling

The neurotransmitters and hormones produced by neurons and immune cells

control exocrine functions. Salivary gland is one of exocrine glands communicating vigorously with other cells. Salivary gland cells are classified as non-excitable cells, as they lack voltage-sensitive channels, and they communicate with other cells through G-protein-coupled receptors (GPCRs). For example, salivary secretion, one of the essential functions of salivary glands, is mediated by the activation of GPCRs and the subsequent increase in cytosolic Ca^{2+} levels ($[Ca^{2+}]_i$) (Roussa, 2011; Lee et al., 2012). Therefore, impairment of GPCR-mediated signaling results in the dysfunction of salivary glands (Jin et al.,2012). In the human salivary gland, a series of GPCRs, including P2Y2, histamine, and S1P have been investigated, elucidating their unique functions (Baker et al., 2008; Kim et al., 2009; Seo et al., 2010).

Neuromuscular junction as another target of peripheral nervous system.
The *Drosophila* neuromuscular junction (NMJ) is a good model system used for the study of synaptic development and plasticity. There are 30 muscles per hemisegment whose arrangement within the peripheral body wall is known. A total of 31 motor axons attach to these muscles in a high fidelity pattern and it forms a synaptic arbor with varicosities, synaptic boutons. This anatomical structure not only facilitates observation of structural changes, but also permits single cell resolution. The advantage is that powerful genetics can control specific genes spatially or temporally. It can also represent the excitatory synapse of the CNS with glutamatergic synapse such as the hippocampus.

Purpose
I studied the regulation by neurotransmitter in peripheral nervous system in two major model systems. I tried to understand the calcium signal by

comparing the characteristics of SOCE, downstream of the intracellular calcium signal of non-excitatory cells, including the human salivary gland. I examined the activity and inhibitory mechanism in the receptor regulation of the salivary gland. I studied ZnR / GPR39 as a new receptor recognition and receptor activity increase study and studied the mechanism of chloropromazine as a receptor inhibition study. In addition, I tried to confirm the role of CRBN-mediated neurotransmitter regulation, which regulates the surface level of the BK channel, downstream of the calcium signal in the PNS. To this end I have studied a physiological role of pathogenic CRBN in *Drosophila* NMJ.
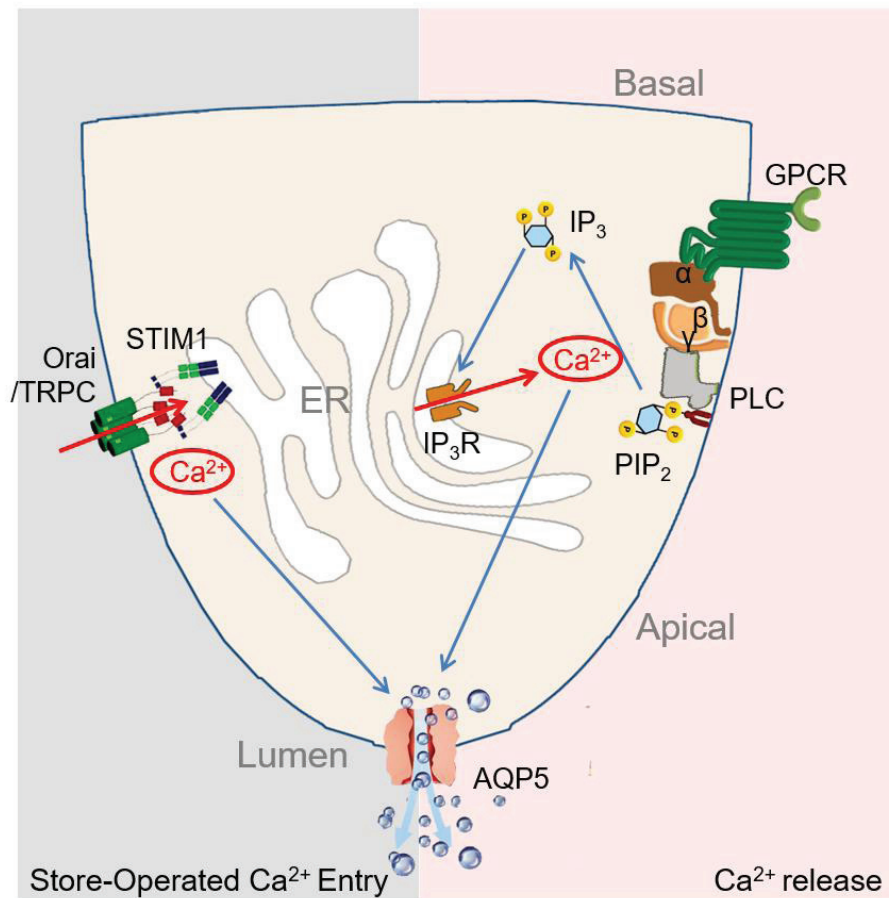
Figure 1. Ca^{2+} signal transduction and regulation of fluid secretion in salivary gland acinar cells. This figure shows the key signaling events and components involved in the regulation of fluid secretion in salivary gland cells. Increase of cytosolic calcium as a result of neurotransmitter stimulation, intracellular Ca^{2+} release and Ca^{2+} influx induces the regulation of ion transport through the apical membrane of cells, the production of osmotic gradient and the flow of water.

CHAPTER I

Characterization of SOCE in non-excitable cells

including salivary gland cells

1.1. Introduction

Recently, a growing number of studies have shown SOCE to be a core step of phospholipase C (PLC) signaling. SOCE is a key mechanism in PLC-mediated Ca^{2+} signaling (Lopez et al., 2016). The IP_3 produced by PLC activity binds to IP_3 receptors in intracellular Ca^{2+} pools (such as ER) and evokes Ca^{2+} release. The consequence of this process is the depletion of intracellular Ca^{2+} pools, which triggers a structural change in STIM1, a Ca^{2+} sensor in Ca^{2+} pools. The activated STIM1 interacts with Orai and/or TRPC in the plasma membrane and initiates Ca^{2+} influx from the extracellular space. Because SOCE helps maintain intracellular Ca^{2+} pools by refilling Ca^{2+} after depletion, SOCE perturbations are an important toxic mechanism. My lab recently reported that NDL-PCBs including PCB19 block Ca^{2+} signaling pathways by SOCE inhibition in neuronal PC12 cells (Choi et al., 2016). NDL-PCBs inhibited thapsigargin-induced Ca^{2+} influx as well as bradykinin receptor-mediated Ca^{2+} signaling.

However, it is not known whether these cells have the same mechanism. Since SOCE requires coordination of several intracellular Ca^{2+} sensors and channels, it is thought that the regulatory mechanisms are different depending on the type of Ca^{2+} sensor and channel involved. In particular, the degree of contribution of SOCE to intracellular calcium signal is predicted to be different between excitable cells (with voltage-sensitive Ca^{2+} channels) and non-excitable cells (dependent only on G-protein coupled receptors). However, studies comparing these characteristics in non-excitatory cells have not been well conducted. For example, neuronal PC12 cells express a series of SOCE-related channels including TRPC (Heo et al., 2012), it was still unclear whether SOCE in PC12 cells is the most common SOCE form

mediated by Orai family. I have described in chapter 3 that chlorpromazine inhibits SOCE. Characterization and comparison of SOCE will provide very important information in predicting how SOCE inhibition of chlorpromazine will appear in other cells and in other ways.

To this end, I characterized SOCE in human submandibular gland HSG cells, rat pheochromocytoma PC12 cells, human embryonic kidney 293 (HEK293) cells (Graham et al., 1977), human leukemia T cell line Jurkat-T cells (Gillis and Watson, 1980), and human promyelocytoma HL-60 cells (Collins et al., 1978). I compared the SOCE of HSG cells with SOCEs of other cells that are good model systems for testing Orai-dependent SOCE because previous literatures have demonstrated that these cell lines intrinsically express Orai channels (DeHaven et al., 2009; Gwozdz et al., 2012; Dörr et al., 2016; Schaff et al., 2010).

1.2. Materials and Methods

Materials

Carbachol, histamine and sulfinpyrazone were purchased from Sigma (St. Louis, MO, USA). 2APB, ML9, Gd^{3+}, and SK&F96365 were obtained from Tocris (Bristol, UK). Thapsigargin was purchased from Alomone Labs (Jerusalem, Israel). Fura-2/acetoxymethylester (Fura-2/AM) was obtained from Molecular Probes (Eugene, OR, USA). Fetal bovine serum, modified Eagle's Medium, RPMI 1640 medium, and penicillin/streptomycin were purchased from Gibco (Grand Island, NY, USA).

Cell culture

PC12, Jurkat T and HL-60 cells were maintained in RPMI 1640 medium supplemented with 10% (v/v) heat-inactivated fetal bovine serum and 1% (v/v) penicillin/streptomycin. HEK293 cells and HSG cells were maintained in Dulbecco's modified Eagle's medium (DMEM) supplemented with 10% (v/v) fetal bovine serum and 1% (v/v) penicillin/streptomycin. The cell line was cultured in a humidified atmosphere of 95% air + 5% CO_2.

Measurement of intracellular Ca^{2+} concentrations ($[Ca^{2+}]_i$)

The fluorescent Ca^{2+} indicator, fura-2, was used to determine $[Ca^{2+}]_i$ according to previously reported methods (Choi et al., 2016). Briefly, cell suspensions were incubated in Locke's solution (154 mM NaCl, 5.6 mM KCl, 10 mM glucose, 2.2 mM $CaCl_2$, 1.2 mM $MgCl_2$, and 5 mM HEPES buffer adjusted to pH 7.4) supplemented with 3 μM fura-2/AM for 50 min at 37 °C with continuous stirring. Fluorescence ratios were monitored using 340 and 380 nm dual excitation wavelengths. The ratio of resultant intensities was

detected at a 500 nm emission wavelength. Fluorescence ratios were converted into $[Ca^{2+}]_i$ as described by Grynkiewicz et $al.,$(1985). Extracellular Ca^{2+}-free solution was 200 μM EGTA-containing Ca^{2+} free Locke's solution (156.2 mM NaCl, 5.6 mM KCl, 1.2 mM $MgCl_2$, 5 mM HEPES, 10 mM glucose, adjusted to pH 7.4). Where indicated, 2.5 mM $CaCl_2$ was added to monitor subsequent Ca^{2+} influx.

Statistical analysis

Data analyses and graphical display were performed with SigmaPlot (Version 11.0, Systat Software, Germany). All displayed values represent the mean ± SEM. Significant differences between groups were determined using independent or paired Student's t-tests or Mann-Whitney U test, and multiple comparisons were performed using two-way ANOVA.

1.3. Results

Since SOCE requires coordination of several intracellular Ca^{2+} sensors and channels, it is expected that the regulatory mechanism will be different depending on the type of Ca^{2+} sensor and channel involved. By confirming the diversity of the SOCE mechanism of these cells, the cell specific SOCE inhibitory effect of various drugs can be expected. Characterization and comparison of SOCE will provide very important information in predicting how SOCE inhibition effects of chlorpromazine identified will appear in other cells and in other ways. To this end, I characterized the SOCE in rat pheochromocytoma PC12 cells, human embryonic kidney 293 (HEK293) cells (Graham et al., 1977), human leukemia T cell line Jurkat-T cells (Gillis and Watson, 1980), and human promyelocytoma HL-60 cells (Collins et al., 1978) as well as HSG cell. These cells are good model systems for testing Orai-dependent SOCE because previous literatures have demonstrated that these cell lines intrinsically express Orai channels (DeHaven et al., 2009; Gwozdz et al., 2012; Dörr et al., 2016; Schaff et al., 2010).

I tested these cell lines with the SOCE inhibitors 1-{-[3-(4-methoxyphenyl) propoxy]-4-methoxyphenyl}-1H-imidazole hydrochloride (SK&F96365, STIM1 inhibitor), Gd^{3+} (known to block Orai channels), and 1-(5-chloronaphthalenesulfonyl) homopiperazine hydrochloride (ML-9, known to act on STIM1) (Parekh, 2010; Salmon et al., 2010). 2-Aminoethyldiphenyl borate (2APB, IP_3 receptor antagonist) also acts as a SOCE inhibitor, although it dilates Orai1 pore size under specific circumstances (Xu et al., 2016). First I analyzed the effect of SOCE inhibitors in PC12 cells. I found that ML-9 induced only marginal inhibition (Fig. 1-1A) and Gd^{3+} almost failed to inhibit SOCE in PC12 cells (Fig. 1-1B),

in which SOCE was clearly different from Orai-dependent SOCE in other cells (Fig. 1-1C). I repeated the same set of experiments in HEK293 cells. I confirmed the previous findings that SOCE in HEK293 cells is sensitive to ML-9 (Fig. 1-2A) (Martin et al., 2009) and Gd^{3+} (Fig. 1-2B) (DeHaven et al., 2009), as well as other SOCE inhibitors (Fig. 1-2C). Moreover, I repeated the same experiments with another Orai-dominant cell lines, HL-60 cells (Fig. 1-3) and Jurkat T (Fig. 1-4). Not only 2APB and SK&F96365, but also Gd^{3+} and ML-9 successfully inhibited thapsigargin-induced Ca^{2+} influx in Jurkat T and HL-60 cells. The same experiment was reproduced in human salivary gland, HSG cells. As a result, the increase of intracellular calcium was inhibited by 2APB, SK&F96365 and ML-9, but no inhibitory effect by Gd^{3+} was observed in HSG cells (Fig. 1-5).

1.4. Discussion

In this study, I first tested whether the SOCEs in PC12, Jurkat T, HL-60, HEK293, and HSG cells were identical and equally sensitive to Orai-mediated SOCE inhibitors such as ML-9 and Gd^{3+}. Surprisingly, I found that SOCE in PC12 and HSG cells, unlike SOCE in the majority of other cell types, is unusually resistant to Gd^{3+} even at 100 μM, a dose which is much higher than the nanomolar-submicromolar concentrations known to block Orai channels. These results suggest that SOCE in PC12 cells and HSG cells is distinct from typical Orai-dependent SOCE. A recent study reported that SOCE inhibition induced by 100 μM Gd^{3+} was about 80% of that induced by SK&F96365 in PC12 cells (Takahashi et al., 2014). PC12 cells express TRPC1-6, and their SOCE has been suggested to be mediated mostly by TRPC channels (Heo et al., 2012), which are well known to mediate Gd^{3+}-insensitive SOCE (DeHaven et al., 2009).

Actually, it is not surprising that there are variations of SOCE with different pharmacological profiles. For example, SOCE in pulmonary artery smooth muscle cells shows Gd^{3+}-sensitivity but 2APB-resistance (McElroy et al., 2009). The SOCE in endothelial colony-forming cells shows different Gd^{3+}-sensitivity according to the SOCE-triggering stimulant such as ATP or cyclopiazonic acid (Dragoni et al., 2014). These differences are not fully understood but are considered to be due to different distributions of SOCE signaling components such as Orai subtype and STIM family.

Orai inhibition is a possible common toxic mechanism in various cell types with Ca^{2+} signaling. Mutant mice with genetic deletion of Orai1 show serious immune dysfunction, tooth malformation, and impaired skin homeostasis (Feske et al., 2009; Vandenberghe et al., 2013). Pharmacological

agents inhibiting Orai are also reported to show high potential for immunotoxicity (Palleschi et al., 2009; Zou et al., 2012; Heo et al., 2015). Orai1, the most studied channel for SOCE, is a transmembrane domain channel that, when activated by STIM1, forms highly Ca^{2+} -selective, inwardly rectifying Ca^{2+} currents (I_{CRAC}) (Hogan et al., 2010; , 2009). While this current is well known in lympocytes and mast cells, it has not yet been measured in salivary ancinar cells. In contrast, a relatively non-selective cation current was observed in the salivary gland cell that is more consistent with the TRPC channel characteristics (Liu et al., 2007). HSG have been shown to express TRPC channels including TRPC1 and TRPC3, contribute to SOCE, and affect fluid secretion (Birnbaumer et al., 1996; Montell. 2005; Liu et al., 2007; Liu et al., 2000; Kim et al., 2011). These results suggest that TRPC may be dominant in the SOCE composition acting on cytosolic Ca^{2+} influx in HSG cells.

A PC12 cells

$[Ca^{2+}]_i$ (nM)

0 mM $[Ca^{2+}]_{external}$

100 sec

Vehicle

ML-9 100 μM

Inhibitor   TG   2.2 mM Ca^{2+}

B

$[Ca^{2+}]_i$ (nM)

Vehicle
Gd^{3+} 10 μM

2APB

Inhibitor   TG   2.2 mM Ca^{2+}

C

$[Ca^{2+}]_i$ rise, % of Control

Vehicle 2APB SKF Gd^{3+} 10 μM Gd^{3+} 100 μM ML-9 100 μM ML-9 300 μM

8   4   4   3   3   3   6

*** *** ** ***

Figure 1-1. Characterization of thapsigargin-induced $[Ca^{2+}]_i$ rise in PC12 cells. **(A-B)** Fura-2-loaded PC12 cells were pretreated with inhibitors in the extracellular Ca^{2+}–free condition, as indicated, and then stimulated with 1 μM thapsigargin in the absence of extracellular Ca^{2+}. Ca^{2+} influx was induced by adding 2.2 mM $CaCl_2$ (Ca^{2+}) into the extracellular space: vehicle (light gray trace in **A** and **B**), 100 μM ML-9 (dark gray trace in **A**), 10 μM GdCl$_3$ (dark gray trace in **B**), and 20 μM 2APB (black trace in **B**). All inhibitors were pretreated 210 sec prior to thapsigargin treatment. TG, thapsigargin. **(C)** Peak levels of thapsigargin-induced $[Ca^{2+}]_i$ influx after $CaCl_2$ treatment were quantitatively analyzed and depicted as % of the thapsigargin-induced $[Ca^{2+}]_i$ rise without inhibitor treatment. SKF, 20 μM SK&F96365. Number of experiments are depicted in bar graph. Each point shown is the mean $\pm$ SEM. $**P < 0.01$; $***P < 0.001$, compared to vehicle control.

A HEK293 cells

0 mM $[Ca^{2+}]_{external}$

100 sec

$[Ca^{2+}]_i$ (nM)

Vehicle

ML-9 100 μM

Inhibitor TG 2.2 mM Ca^{2+}

B

$[Ca^{2+}]_i$ (nM)

Vehicle
2APB
Gd^{3+} 10 μM

Inhibitor TG 2.2 mM Ca^{2+}

C

$[Ca^{2+}]i$ rise, % of Control

Vehicle 2APB SKF Gd^{3+} 10 μM ML-9 100 μM

20

Figure 1-2. Characterization of thapsigargin-induced $[Ca^{2+}]_i$ rise in HEK293 cells. **(A-B)** Fura-2-loaded HEK293 cells were pretreated with the inhibitors in the extracellular Ca^{2+}–free condition, as indicated, and then stimulated with 1 μM thapsigargin in the absence of extracellular Ca^{2+}. Ca^{2+} influx was induced by adding 2.2 mM $CaCl_2$ (Ca^{2+}) into the extracellular space: vehicle (light gray trace in **A** and **B**), 100 μM ML-9 (dark gray trace in **A**), 10 μM $GdCl_3$ (dark gray trace in **B**), and 20 μM 2APB (black trace in **B**). All inhibitors were pretreated 210 sec prior to thapsigargin treatment. TG, thapsigargin. **(C)** Peak levels of thapsigargin-induced $[Ca^{2+}]_i$ influx after $CaCl_2$ treatment were quantitatively analyzed and depicted as % of the thapsigargin-induced $[Ca^{2+}]_i$ rise without inhibitor treatment. SKF, 20 μM SK&F96365. Number of experiments are depicted in bar graph. Each point shown is the mean ± SEM. **$*P < 0.01$, compared to vehicle control.

A HL-60 cells

$[Ca^{2+}]_i$ (nM)

0 mM $[Ca^{2+}]_{external}$

100 sec

Vehicle

ML-9 100 μM

Inhibitor   TG   2.2 mM Ca^{2+}

B

$[Ca^{2+}]_i$ (nM)

Vehicle

Gd^{3+} 30 μM

2APB

Inhibitor   TG   2.2 mM Ca^{2+}

C

$[Ca^{2+}]_i$ rise, % of Control

Vehicle   2APB   SKF Gd^{3+} 10 μM Gd^{3+} 30 μM Gd^{3+} 100 μM   ML-9 100 μM

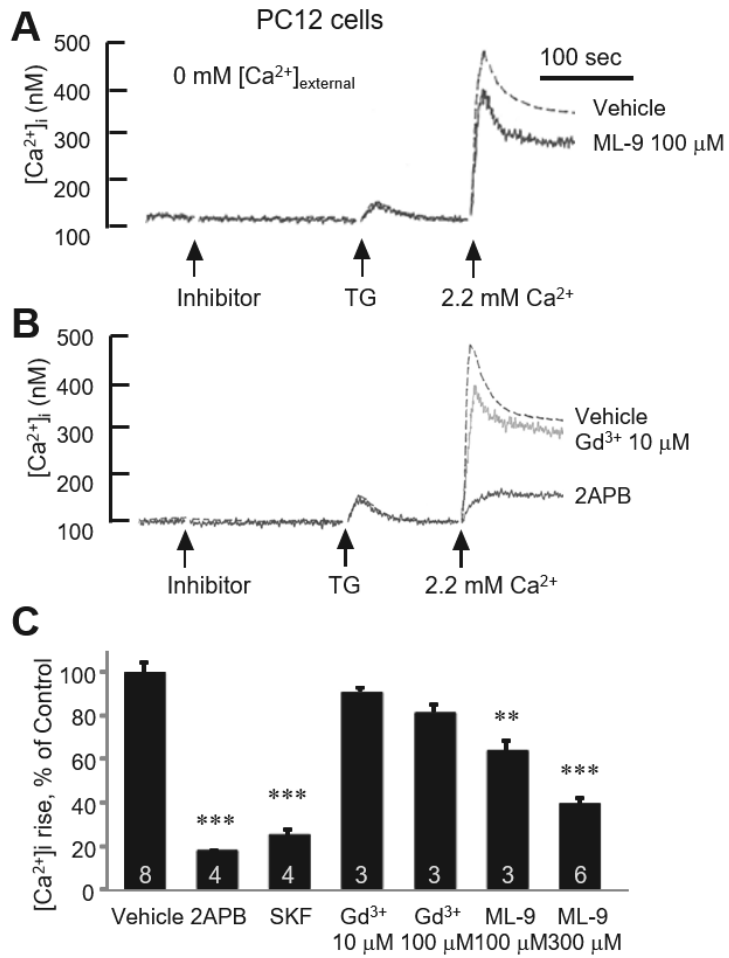6   4   4   4   5   4   3

***   ***   ***   ***   ***

Figure 1-3. Characterization of thapsigargin-induced $[Ca^{2+}]_i$ rise in HL-60 cells. **(A-B)** Fura-2-loaded HL-60 cells were pretreated with the inhibitors in the extracellular Ca^{2+}–free condition, as indicated, and then stimulated with 1 μM thapsigargin in the absence of extracellular Ca^{2+}. Ca^{2+} influx was induced by adding 2.2 mM $CaCl_2$ (Ca^{2+}) into the extracellular space: vehicle (light gray trace in **A** and **B**), 100 μM ML-9 (dark gray trace in **A**), 10 μM $GdCl_3$ (dark gray trace in **B**), and 20 μM 2APB (black trace in **B**). All inhibitors were pretreated 210 sec prior to thapsigargin treatment. TG, thapsigargin. **(C)** Peak levels of thapsigargin-induced $[Ca^{2+}]_i$ influx after $CaCl_2$ treatment were quantitatively analyzed and depicted as % of the thapsigargin-induced $[Ca^{2+}]_i$ rise without inhibitor treatment. SKF, 20 μM SK&F96365. Number of experiments are depicted in bar graph. Each point shown is the mean $\pm$ SEM. ***$P < 0.001$, compared to vehicle control.

A Jurkat T cells
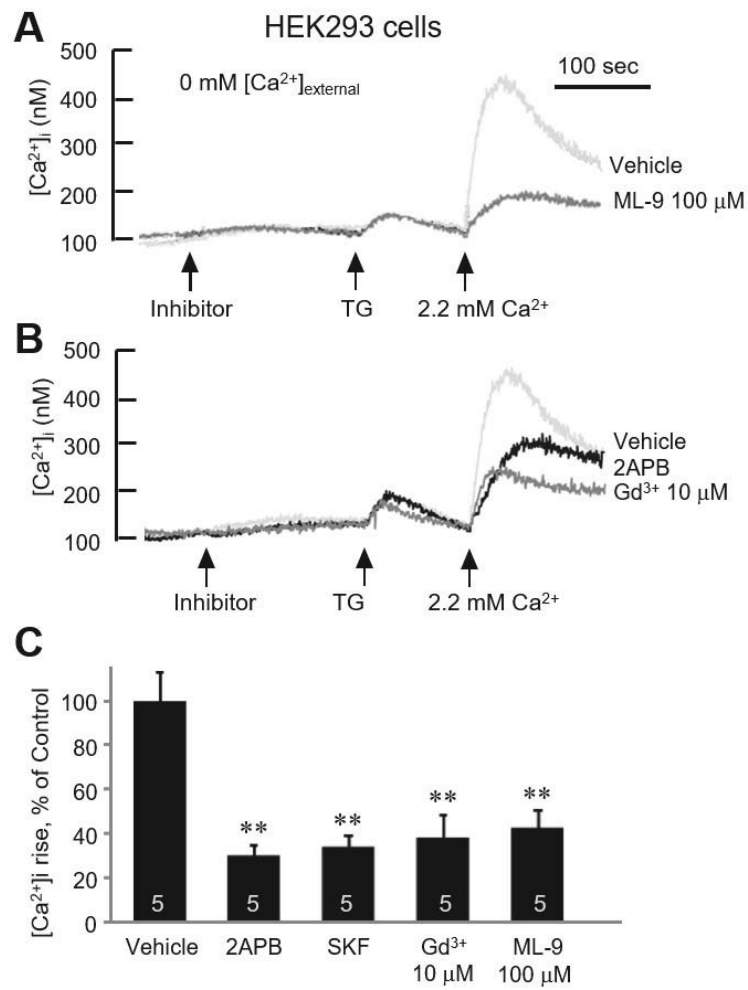
0 mM [Ca^{2+}]$_{external}$

100 sec

Vehicle

ML-9 100 µM

Inhibitor TG 2.2 mM Ca^{2+}

B

Vehicle

Gd^{3+} 30 µM
2APB

Inhibitor TG 2.2 mM Ca^{2+}

C

[Ca^{2+}]i rise, % of Control

Vehicle | 2APB | SKF | Gd^{3+} 10 µM | Gd^{3+} 30 µM | ML-9 100 µM

9 4 5 3 4 6

*** *** *** ***

Figure 1-4. Characterization of thapsigargin-induced $[Ca^{2+}]_i$ rise in Jurkat T cells. **(A-B)** Fura-2-loaded Jurkat T cells were pretreated with the inhibitors in the extracellular Ca^{2+}–free condition, as indicated, and then stimulated with 1 μM thapsigargin in the absence of extracellular Ca^{2+}. Ca^{2+} influx was induced by adding 2.2 mM $CaCl_2$ (Ca^{2+}) into the extracellular space: vehicle (light gray trace in **A** and **B**), 100 μM ML-9 (dark gray trace in **A**), 10 μM $GdCl_3$ (dark gray trace in **B**), and 20 μM 2APB (black trace in **B**). All inhibitors were pretreated 210 sec prior to thapsigargin treatment. TG, thapsigargin. **(C)** Peak levels of thapsigargin-induced $[Ca^{2+}]_i$ influx after $CaCl_2$ treatment were quantitatively analyzed and depicted as % of the thapsigargin-induced $[Ca^{2+}]_i$ rise without inhibitor treatment. SKF, 20 μM SK&F96365. Number of experiments are depicted in bar graph. Each point shown is the mean ± SEM. ***$P < 0.001$, compared to vehicle control.
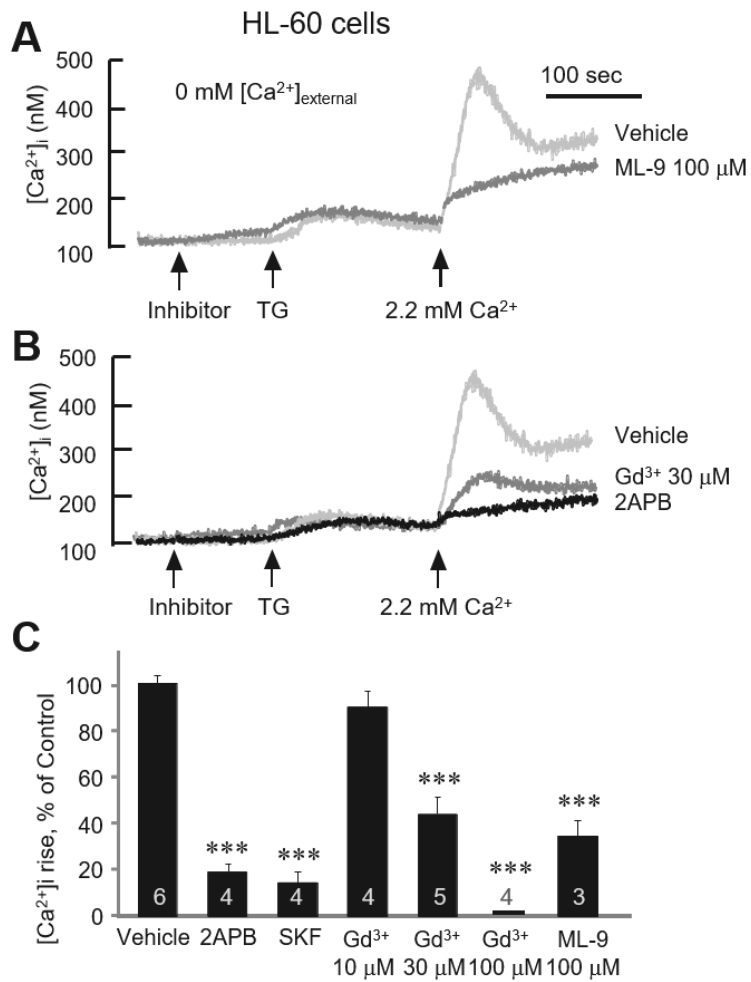
A HSG cells

200 sec

0 mM $[Ca^{2+}]_{external}$

$[Ca^{2+}]_i$ (nM)

Vehicle
SKF

↑ Inhibitor   ↑ TG   ↑ 2.2 mM Ca^{2+}

B

$[Ca^{2+}]_i$ (nM)

Vehicle
ML-9 100 μM

↑ Inhibitor   ↑ TG   ↑ 2.2 mM Ca^{2+}

C

$[Ca^{2+}]_i$ rise, % of Control

Vehicle | 2APB | SKF | Gd³⁺ 10 μM | Gd³⁺ 30 μM | Gd³⁺ 100 μM | ML-9 100 μM

4 | 5 | 5 | 3 | 3 | 3 | 3

*** *** ***

Figure 1-5. Characterization of thapsigargin-induced $[Ca^{2+}]_i$ rise in HSG cells. **(A-B)** Fura-2-loaded HSG cells were pretreated with the inhibitors in the extracellular Ca^{2+}–free condition, as indicated, and then stimulated with 1 μM thapsigargin in the absence of extracellular Ca^{2+}. Ca^{2+} influx was induced by adding 2.2 mM $CaCl_2$ (Ca^{2+}) into the extracellular space: vehicle (light gray trace in **A** and **B**), 100 μM ML-9 (dark gray trace in **A**), 10 μM $GdCl_3$ (dark gray trace in **B**), and 20 μM 2APB (black trace in **B**). All inhibitors were pretreated 210 sec prior to thapsigargin treatment.. TG, thapsigargin. **(C)** Peak levels of thapsigargin-induced $[Ca^{2+}]_i$ influx after $CaCl_2$ treatment were quantitatively analyzed and depicted as % of the thapsigargin-induced $[Ca^{2+}]_i$ rise without inhibitor treatment. SKF, 20 μM SK&F96365. Number of experiments are depicted in bar graph. Each point shown is the mean ± SEM. ***$P < 0.001$, compared to vehicle control.
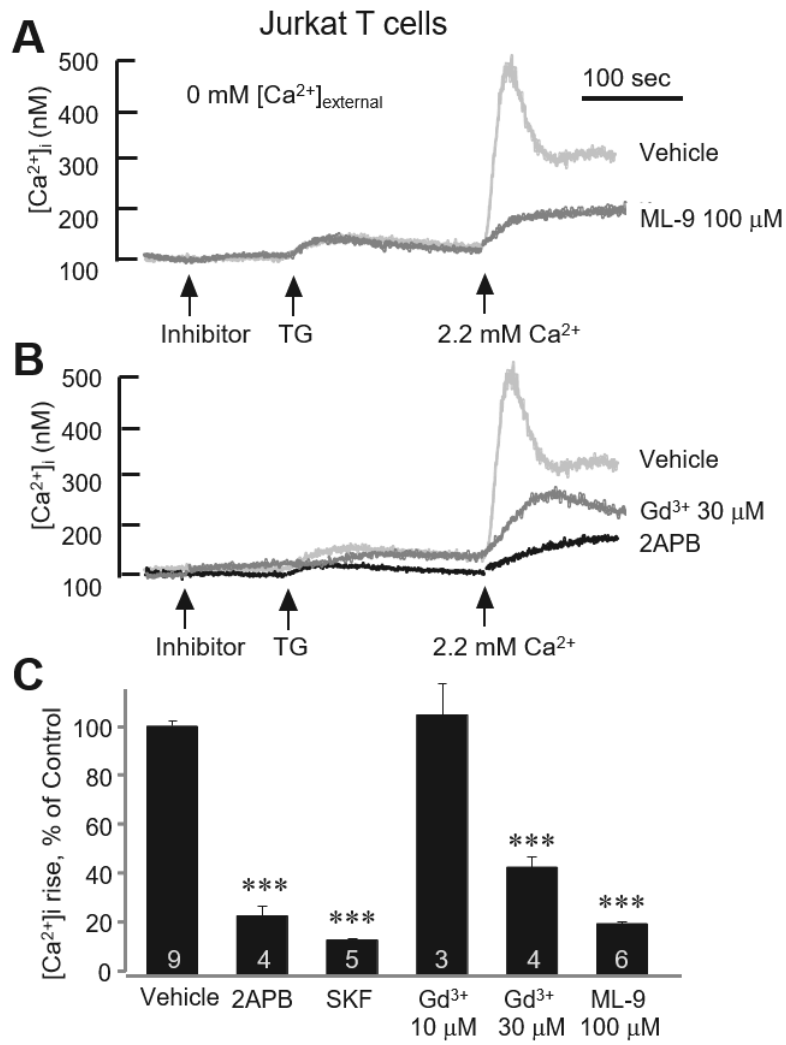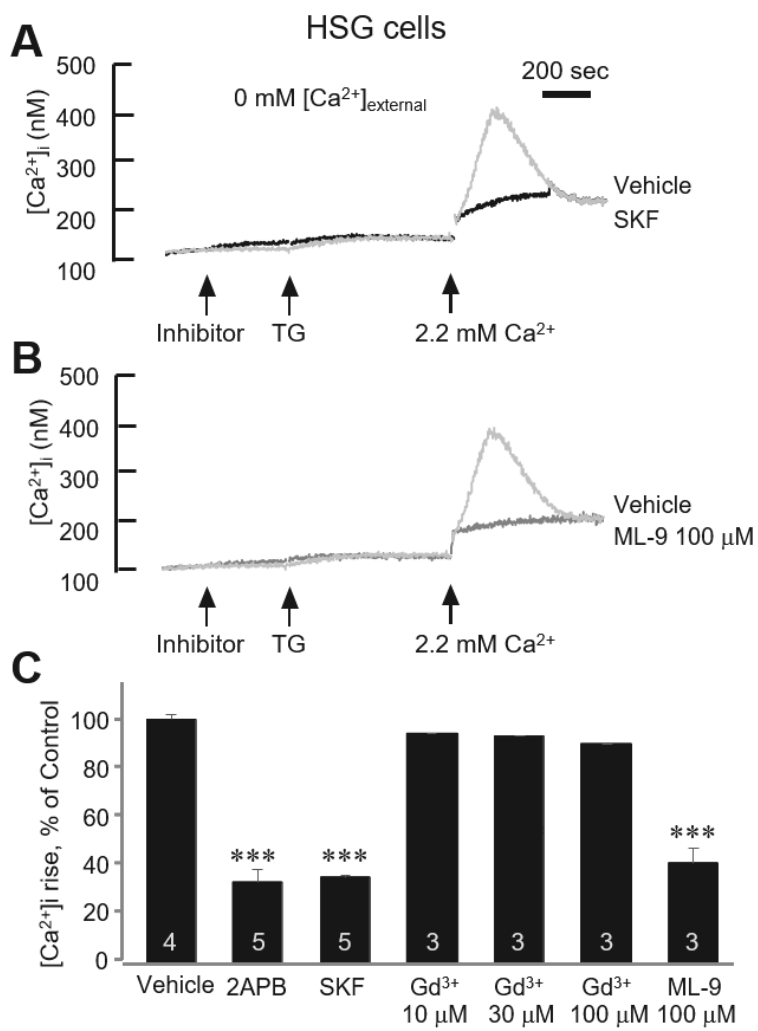
CHAPTER II

ZnR/GPR39 signaling-mediated salivary secretion

2.1. Introduction

Zn^{2+} is a divalent cation that acts as a cofactor of various enzymes (Vallee and Falchuk, 1993). Zn^{2+}, which binds to many proteins and regulates their function, plays an important physiological role in many cells including neurons (Sensi et al., 2011; Sekler and Silverman, 2012). Since Zn^{2+} acts like a second messenger and releases into the extracellular space by cell death, the cells have Zn transporters to utilize Zn^{2+} (Sekler et al., 2007). Extracellular Zn^{2+} modulates cellular activity by regulating channels such as the NMDA receptor, GABA receptor, and purinoceptor (Peralta and Huidobro-Toro, 2016). In addition, Zn^{2+} can also act by G-protein coupled receptors that selectively recognize Zn^{2+}. Metabotropic Zn receptors, also known as GPR39, are present in hippocampal neurons, keratinocytes, colon epithelial cells, and pancreatic cells (Hershfinkel, 2018). ZnR / GPR39 activates phospholipase C as a Gq-coupled receptor and induces cytosolic Ca^{2+} signaling by forming intracellular IP_3 (Hershfinkel et al., 2001).

As I reviewed in the previous chapter, intracellular calcium is a major factor controlling salivation in salivary glands (Ambudkar, 2016). Acetylcholine secreted from parasympathetic neurons acts on the muscarinic receptors of salivary gland membranes to induce a salivary secretion by inducing phospholipase C-dependent cytosolic Ca^{2+} increase (Proctor, 2016). Muscarinic receptors, as well as histamine receptors in salivary glands, induce intracellular calcium and salivary secretion in a Gq-coupled receptor- and phospholipase C-dependent manner (Kim et al., 2009). Therefore, the Gq coupled receptor present in the salivary gland may be an important salivary control factor.

Interestingly, it was found that ZnR/GPR39 is expressed in HSY cells, a human submandibular ductal cell line, leading to a Zn^{2+} -induced Ca^{2+} increase (Sharir and Hershfinkel, 2005). In addition, the interaction of ZnR with another G-protein-coupled receptor, CaSR, has also been identified (Asraf et al., 2014). However, the mechanism of salivary secretion by Zn^{2+} and ZnR/GPR39 has not been elucidated, although it is clear that salivary Ca^{2+} signaling is associated with salivation. Since $ZnCl_2$ is commonly used to remove bad breath (Kang et al., 2017; Suzuki et al., 2018), it is a very interesting attempt to determine the mechanism of Zn secretion regulation.

In this study, I investigated the expression of ZnR in human submandibular gland cells, and investigated the mechanism of intracellular uptake and the effect of Zn^{2+} on salivary secretion by examining the aquaporin-5 translocation by Zn^{2+}.

2.2. Materials and Methods

Materials

Zinc, Carbachol, histamine and sulfinpyrazone were purchased from Sigma (St. Louis, MO, USA). Pirenzepine, Chlorpheniramine, U73122 and 2APB were obtained from Tocris (Bristol, UK). Thapsigargin was purchased from Alomone Labs (Jerusalem, Israel). Fura-2/acetoxymethylester (Fura-2/AM) was obtained from Molecular Probes (Eugene, OR, USA). Fetal bovine serum, modified Eagle's Medium, and penicillin/streptomycin were purchased from Gibco (Grand Island, NY, USA). Myc tagged AQP5 construct was purchased from Origene (Rockville, MD, USA).

Cell culture

HSG cells were maintained in Dulbecco's modified Eagle's medium (DMEM) supplemented with 10% heat-inactivated fetal bovine serum and 1% penicillin/streptomycin. The cell line was cultured in a humidified atmosphere of 95% air + 5% CO_2. The culture medium was changed every day, and the cell lines were subcultured every 3 day.

Measurement of intracellular Ca^{2+} concentrations ($[Ca^{2+}]_i$)

The fluorescent Ca^{2+} indicator, fura-2, was used to determine $[Ca^{2+}]_i$ according to previously reported methods (Choi et al., 2016). Briefly, cell suspensions were incubated in Locke's solution (154 mM NaCl, 5.6 mM KCl, 5.6 mM glucose, 2 mM $CaCl_2$, 2 mM $MgCl_2$, and 5 mM HEPES buffer adjusted to pH 7.4) supplemented with 3 μM fura-2/AM for 50 min at 37 °C with continuous stirring. Fluorescence ratios were monitored using 340 and 380 nm dual excitation wavelengths. The ratio of resultant intensities was

detected at a 500 nm emission wavelength. Extracellular Ca^{2+}-free solution was 200 μM EGTA-containing Ca^{2+} free Locke's solution (156.2 mM NaCl, 5.6 mM KCl, 1.2 mM $MgCl_2$, 5 mM HEPES, 10 mM glucose, adjusted to pH 7.4). Where indicated, 2.5 mM $CaCl_2$ was added to monitor subsequent Ca^{2+} influx.

Immunofluorescent staining

HSG cells were fixed (4% paraformaldehyde), permeabilized (0.5% Triton X-100) for 10 min at 20–25°C, and then incubated for 1 hr in blocking solution (1% bovine serum albumin). Primary antibodies were challenged for overnight (at 4 °C), and then incubated with secondary antibodies for 1 hr (at room temperature). The following primary antibodies were used: NLS142 (NOVUS) for anti-human GPR39, 2276 (Cell Signaling) for anti-Myc and sc9891 (Santa cruz Biotechnology) for anti-AQP5 channels. Secondary antibody incubations were carried out for 1 h at room temperature using Cy3-conjugated goat anti-rabbit IgG (1:500; Invitrogen, Carlsbad, CA, USA) antibodies.

Cell Transfection and Quantification of Surface AQP5 channels

Cells were transfected using Lipofectamine 2000 (Invitrogen), according to the manufacturer's instructions. For fluorescence-based measurements of cell-surface AQP5, HSG cells transfected with pCMV6-AQP5-Myc construct were incubated for 16 hrs. Cells were fixed in PBS containing 4% formaldehyde and stained for surface AQP5 population using goat anti-AQP5 antibody (1:100, Santa Cruz) in PBS under non-permeable condition for overnight at 4 ℃. Cells were washed three times with PBS and subsequently, cells were permeabilized in PBS containing 0.5% Triton X-100 for 10 min

and stained for total Myc-AQP5 population using mouse anti-Myc antibody (1:100, Cell Signaling) for 1 hr at room temperature and then a Cy3-conjugated anti-goat secondary and Axea488-conjugated anti-mouse secondary antibody (1:500, Jackson ImmunoResearch Laboratories) for 30 min. Images were acquired with a LSM 700 laser-scanning confocal microscope (Carl Zeiss) using C-Apo 40 × 1.20 W objective lens. Cells were outlined, and mean fluorescence intensities measured for each channel using the ZEN imaging software (Carl Zeiss). For quantification of surface AQP5-Myc levels, the fluorescence intensity of surface AQP5 (red) was divided by total AQP5 (green) fluorescence intensity. The ratios of surface-to-total AQP5 fluorescence intensities were compared between vehicle-treated controls

.

Cell surface biotinylation

Biotinylation assays were performed using HSG cells transfected with pCMV6-AQP5-Myc construct. Cells were stimulated with 100 μM Zn (30 minutes at 37 °C) in Locke's solution. To biotinylate the cell surface proteins, cells were labeled with 1.5 mg/ml sulfo-NHS-SS-biotin (Thermo Scientific, 21331) at 4 °C for 20 minutes. Following biotin labeling HSG cells were washed with respective buffer containing 100 mM glycine, and lysed with RIPA buffer. The lysates were then centrifuged at 14,000x g for 15 min at 4 °C and supernatant was collected. Protein concentrations were determined using the BCA Protein Assay Kit (Thermo Scientific, 23225) and biotinylated proteins were pulled down by incubating with NeutrAvidin agarose resins (Thermo Scientific, 29200) for overnight at 4 °C with an end to end rotation. The beads were then washed and the bound proteins were eluted by boiling in SDS dye. The eluted material was analyzed by western blotting.

Statistical analysis

Data analyses and graphical display were performed with SigmaPlot (Version 11.0, Systat Software, Germany). All displayed values represent the mean ± SEM. Significant differences between groups were determined using independent or paired Student's t-tests or Mann-Whitney U test, and multiple comparisons were performed using two-way ANOVA.

2.3. Results

2.3.1. Zn^{2+} increases intracellular Ca^{2+} level in HSG cells.

I wanted to investigate the function of Zn^{2+} in regulating intracellular calcium signaling. Zn^{2+} triggers the intracellular calcium of Fura-2-loaded HSG cells in a concentration-dependent manner (Fig. 2-1). This means that Zn^{2+} can regulate the intracellular calcium of the human salivary gland by itself. So, I wanted to know what kind of GPCR is involved in this signaling. Previous studies have shown that ZnR/GPR39 is present in HSY cells by ZnR and that Zn increases calcium (Sharir and Hershfinkel, 2005). However, it is not known at all what pathway the Zn controls the function of the salivary gland cell.

2.3.2. Zinc inhibits following M3 or H1 signaling in a concentration dependent manner.

I confirmed the expression of ZnR in HSG cells (Fig. 2-2). Since it is known that ZnR can regulate the activity of other GPCRs such as CaSR, I investigated whether Zn^{2+} affects muscarinic receptor or histamine receptor-dependent Ca^{2+} signaling. Interestingly, pretreatment of Zn^{2+} inhibited muscarinic-induced Ca^{2+} signaling, confirming that it acts in a concentration-dependent manner (Fig. 2-3A & B). Similar inhibitory effects were observed in histamine-induced Ca^{2+} signaling (Fig. 2-3C & D). These inhibitory effects of other GPCR-mediated Ca^{2+} signaling by Zn^{2+} can occur at the receptor level or downstream.

2.3.3. Muscarinic antagonist and histamine antagonist fail to block Zn-induced Ca^{2+} signaling.

It was found that the intracellular calcium level by muscarinic receptor and histamine receptor were inhibited by Zn^{2+}, whereas Zn^{2+} itself separately increase $[Ca^{2+}]_i$ level. To confirm inhibition at the receptor level, I tested whether muscarinic antagonists affect Zn-induced Ca^{2+} signaling. Pretreatment of muscarinic receptor antagonist, pirenzepine, strongly inhibited intracellular calcium increase by carbachol, whereas it failed to affect Zn-mediated increase in intracellular calcium (Fig. 2-4), implying that Zn-induced $[Ca^{2+}]_i$ shows muscarinic receptor-independent manner. Similarly, pretreatment of the histamine receptor antagonist, chlorphenamine, strongly inhibited the increase of intracellular calcium by histamine, but the response to Zn^{2+} was not affected (Fig. 2-5). These results suggest that the increase in intracellular calcium via Zn^{2+} was completely distinct from the muscarinic & histamine signal, confirming that it was mediated by another GPCR (possibly ZnR/GPR39).

2.3.4. The PLC-β-linked Zn receptor shares its Ca^{2+} signaling with muscarinic and histamine receptors in HSG cells.

I investigated whether the inhibitory effect of Zn on other GPCR-mediated $[Ca^{2+}]_i$ was derived from the downstream PLC pathway. The PLC-β blocker, U73122, not only completely inhibited muscarinic or histamine-mediated Ca^{2+} signaling (Fig. 2-6), but also inhibited Zn-mediated Ca^{2+} signaling (Fig. 2-7). The results imply the heterologous desensitization, the reduced signal transduction of a particular receptor by other neurotransmitters sharing the same downstream signaling pathway. Muscarinic receptors and histamine receptors in salivary glands are known to induce increased intracellular calcium and salivary secretion in a Gq-coupled receptor- and phospholipase C-dependent manner. Therefore, it was confirmed that when the carbachol and

histamine were treated at different time intervals, they also showed a heterologous desensitization manner (Fig. 2-9). To test the heterologous desensitization between Zn and carbachol, treatment with 300 μM carbachol after pretreatment with 30 μM $ZnSO_4$ significantly reduced carbachol-mediated intracellular Ca^{2+} increase (Fig. 2-8A). The results were similar even if the order was reversed (Fig. 2-8B). In addition, the increase in intracellular calcium via 100 μM histamine was inhibited by pretreatment of Zn^{2+}, and the reverse order also shows the same result (Fig. 2-8C & D). As a result, intracellular calcium signaling by Zn shares a downstream PLC-β with a salivary GPCR such as muscarnic and histamine receptor in HSG cells.

2.3.5. Zn^{2+} shows the modulation on SOCE.

It is reported that SOCE is activated when the calcium in ER is depleted due to PLC-dependent increase of IP_3. I tested whether the increase of intracellular Ca^{2+} by Zn to be related to SOCE. It was found that the intracellular calcium by Zn was remarkably decreased by 2-Aminoethyldiphenyl borate (2-APB) treatment, SOCE inhibitor (Fig. 2-7). Therefore, the increase of Zn-induced $[Ca^{2+}]_i$ is achieved through SOCE.

In the previous results, I confirmed that heterologous desensitization between muscarinic and/or histamine and metabotropic Zn receptor. I tried to examine whether these effects were related to SOCE regulation. The increase in intracellular Ca^{2+} concentration through pretreatment of Zn^{2+} did not show a large change when Zn^{2+} was low (1 ~ 10 μM), whereas Zn^{2+} inhibited SOCE in high concentration (30 μM ~) (Fig. 2-10A & B). In addition, SOCE inhibition was observed (Fig. 2-10C, D) even after pretreatment or post-treatment of Zn^{2+} with free extracellular Ca^{2+}. This means that Zn^{2+} modulates various processes in the regulation of intracellular Ca^{2+} levels.

2.3.6. Zn²⁺ itself increases surface expression of aquaporin-5 in the plasma membrane.

In salivary gland cells, intracellular calcium increase via a variety of mechanisms ultimately triggers the translocation of AQP5, the water channel, causing water secretion. To investigate whether intracellular calcium increase via Zn^{2+} regulates salivation, I confirmed the change of the surface-to-total AQP5 ratio after Zn treatment.

After 30 minutes of 100 μM Zn pretreatment, HSG cells were fixed and anti-AQP5 was binding to the cell surface-AQP5. After washing several times, the cells were permeabilized with PBT and bound to total AQP5 in the whole cell area with another antibody. As a result, the surface-to-total AQP5 ratio was significantly increased after Zn treatment (Fig. 2-11A, B). In addition, I tried to test the Zn^{2+}-induced aquaporin-5 translocation with surface protein-labeling method with biotin. I could confirm that Zn successfully increase the biotinylated aquaporin-5 level in the plasma membrane (Fig. 2-11C). The results strongly suggest the cellular mechanism for Zn-induced salivary secretion.

2.4. Discussion

I have shown that Zn^{2+} activates ZnR/GPR39 expressed in human salivary gland cells, thereby increasing intracellular calcium and inducing translocation of aquaporin-5. Although ZnR/GPR39 has been shown to be expressed in the HSY cell line and many studies have been conducted on the inhibitory potential for halitosis with Zn^{2+}, it was not clear whether salivary ZnR/GPR39 is associated with salivation. In this chapter, I have shown that Zn^{2+} induces phospholipase C dependent Ca^{2+} signaling via the ZnR/GPR39 receptor, which is completely independent of the histaminergic receptor and muscarinic receptors that induce the dominant salivary secretion. I also found that the membrane surface expression of aquaporin-5 was increased by ZnR/GPR39, providing strong cellular and molecular evidence that it would be involved in the mechanism of salivation by Ca^{2+}. My study suggests a new mechanism of action of Zn^{2+} prescribing for halitosis and at the same time re-examines the therapeutic potential of Zn^{2+} for xerostomia and its related oral disease. In particular, the applicability to Sjogren's syndrome-mediated xerostomia is noteworthy. Secretory dysfunction in primary Sjogren's syndrome has been suggested as an autoantibody to muscarinic receptors (Kim et al., 2015; Namkoong et al., 2017). ZnR/GPR39 induces salivary secretion independent of muscarinic signaling and may be a therapeutic alternative to xerostomia due to Sjogren's syndrome.
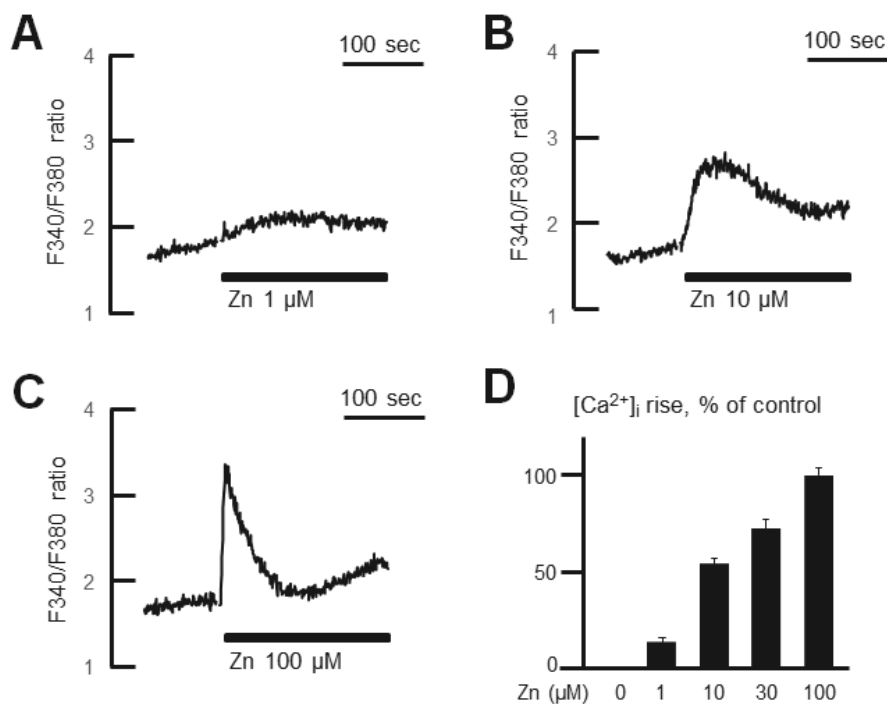
Figure 2-1. Zn-induced changes in intracellular Ca^{2+} concentration in human submandibular gland cells. (A-C) Fura-2-loaded HSG cells were challenged with Zn at various concentrations (1, 10, 100 µM), and then monitored for changes in the fluorescence ratio of F340/F380 as cytosolic [Ca^{2+}] level. (D) Quantification of intracellular Ca^{2+} level was normalized to the level of the group with 100 µM Zn treatment (saturation concentration).
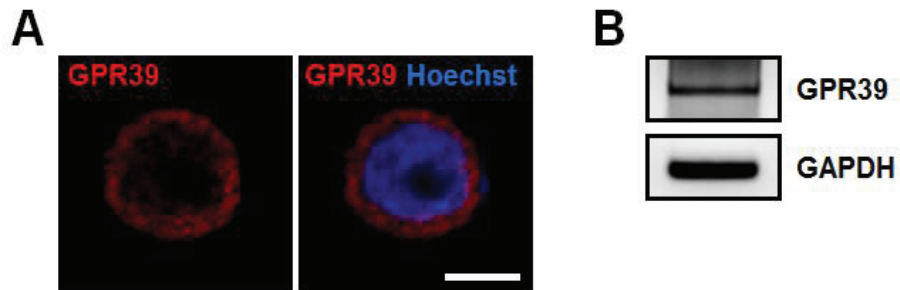
Figure 2-2. ZnR/GPR39 is expressed in HSG cells. (A) Confocal images of HSG cells stained with anti-ZnR (red) and Hoechst (blue). Scale bar: 5 µm. (B) RNA extracted from HSG cells was reverse transcribed into cDNA and amplification reactions were performed using GPR39-specific primers. Glyceraldehyde-3-phosphate dehydrogenase (GAPDH) was used as an internal loading control.
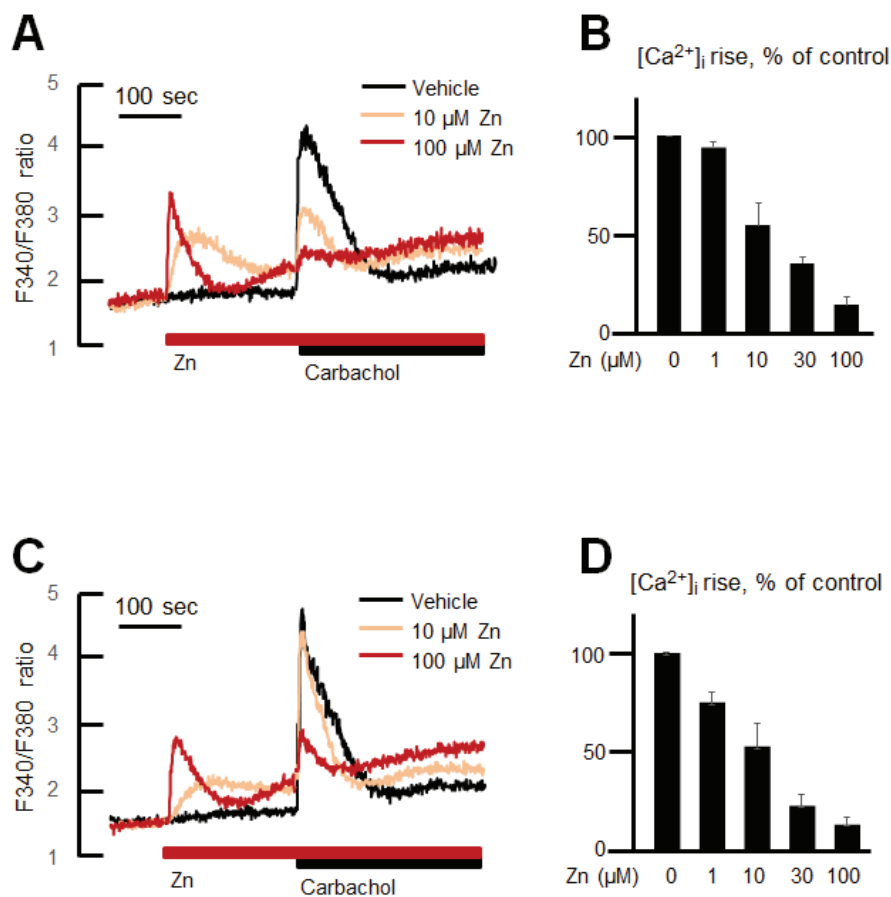
Figure 2-3. Zinc pretreatment inhibits carbachol & histamine-mediated increases in intracellular calcium levels by concentration-dependent manners. (A&C) Fura-2-loaded HSG cells were pretreated with Zn at various concentrations (100 µM, red; 10 µM, pink; vehicle, black), stimulated with 300 µM carbachol (A) or 100 µM histamine (C), and the change in fluorescence ratio of F340 / F380 was monitored at $[Ca^{2+}]_i$ level. (B&D) Quantification of zinc inhibition on intracellular calcium levels mediated by carbachol (B) or histamine (D) was normalized to vehicle groups.
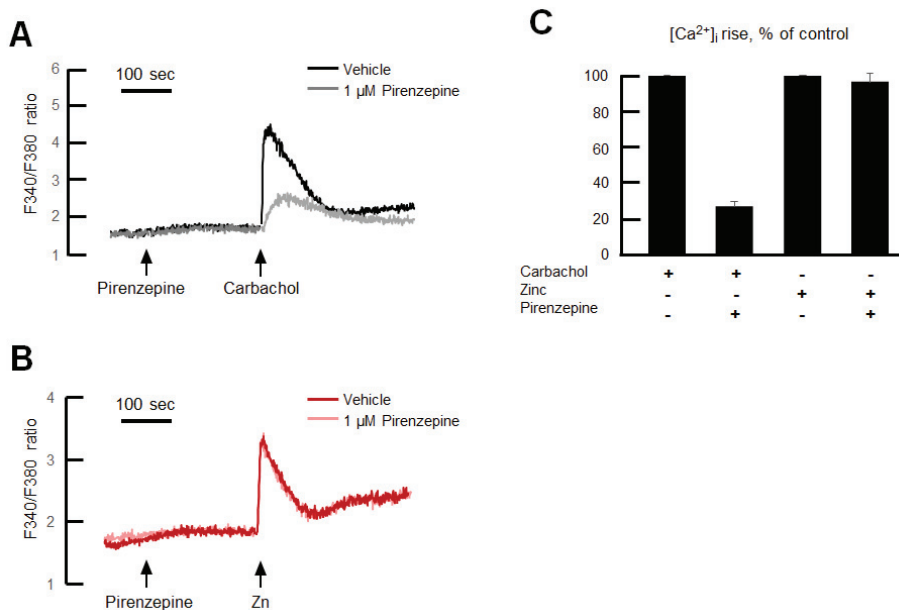
Figure 2-4. The PLC-β-linked Zn signal does not share its Ca^{2+} signaling with muscarinic receptors in HSG cells. (A) Fura-2-loaded HSG cells were treated with 300 μM carbachol with (light gray) or without (black) the pre-incubated 1 μM pirenzepine. (B) HSG cells were treated with 30 μM Zn carbachol with (pink) or without (red) the pre-incubated 1 μM pirenzepine. (C) Quantification of pirenzepine inhibition on intracellular calcium levels mediated by carbachol or zinc was normalized to vehicle groups.

Figure 2-5. The PLC-β-linked Zn signal does not share its Ca^{2+} signaling with histamine receptors in HSG cells. (A) Fura-2-loaded HSG cells were treated with 100 μM histamine with (light gray) or without (black) the pre-incubated 3 μM chlorphenamine. (B) HSG cells were treated with 30 μM Zn carbachol with (pink) or without (red) the pre-incubated 3 μM chlorphenamine. (C) Quantification of chlorphenamine inhibition on intracellular calcium levels mediated by histamine or zinc was normalized to vehicle groups.
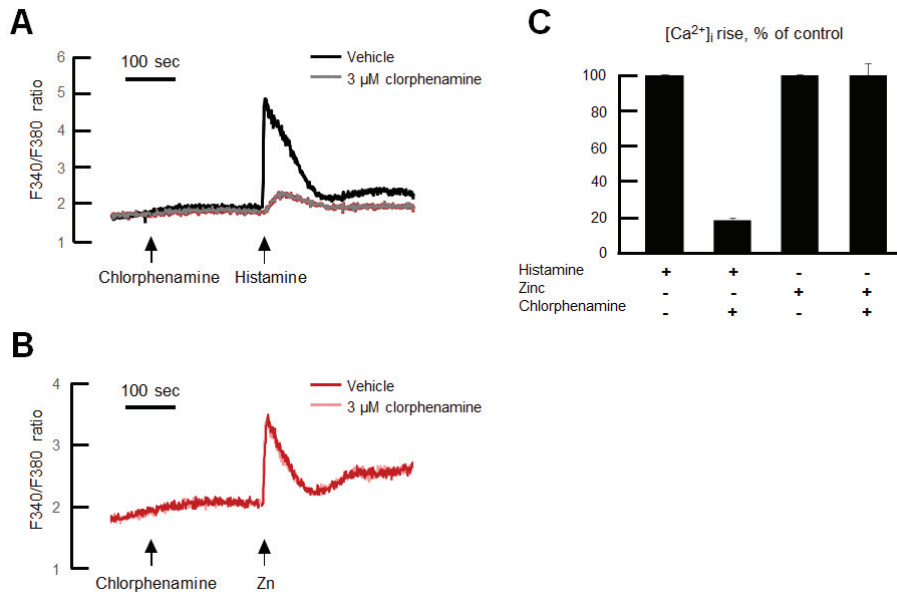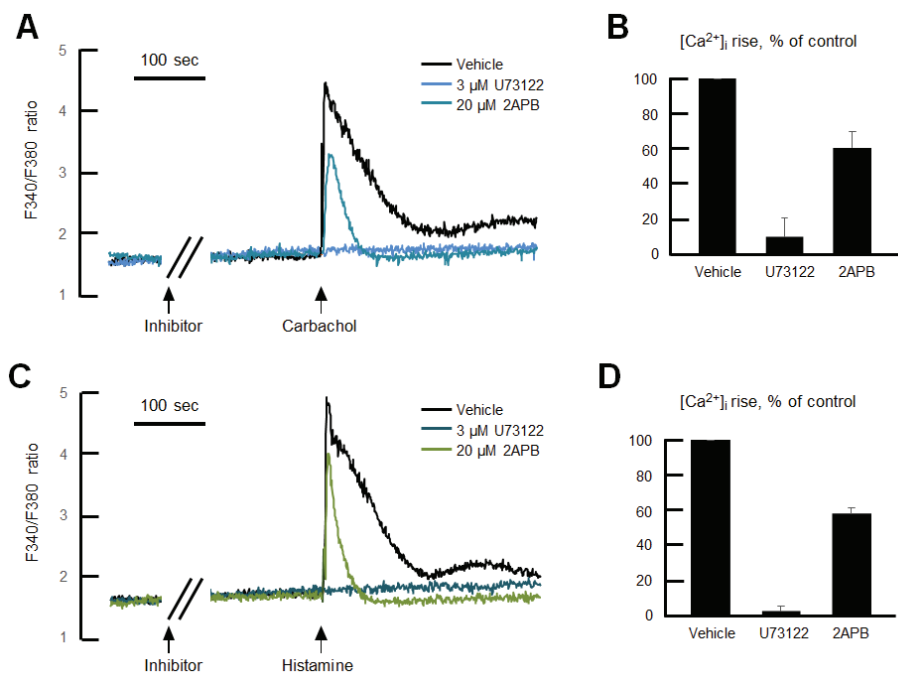
Figure 2-6. The intracellular calcium level regulations of carbachol and histamine are dependent on PLC-β in HSG cells. (A) Fura-2-loaded HSG cells were treated with 300 μM carbachol with (U73122, light blue; 2APB, blue) or without (black) the pre-incubated 3 μM U73122 or 20 μM 2APB. (B) Quantification of the inhibitory effect of U73122 or 2APB on muscarinic-induced intracellular calcium increase. (C) Fura-2-loaded HSG cells were treated with 100 μM histamine with (U73122, green; 2APB, light green) or without (black) the pre-incubated 3 μM U73122 or 20 μM 2APB. (D) Quantification of the inhibitory effect of U73122 or 2APB on histamine-mediated intracellular calcium increase.
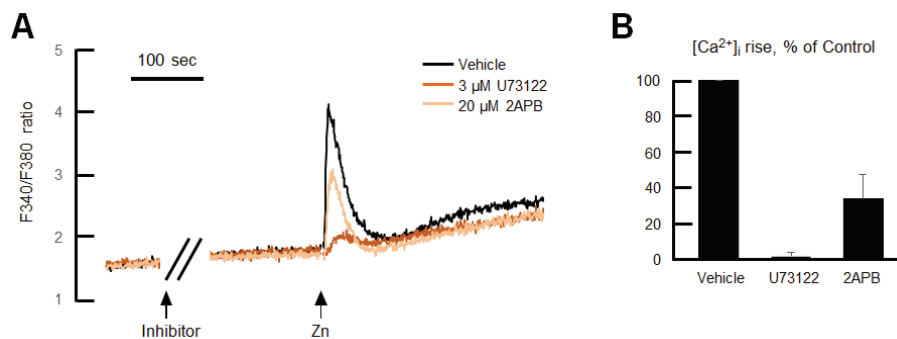
Figure 2-7. The intracellular calcium level regulation of zinc is dependent on PLC-β in HSG cells. (A) Fura-2-loaded HSG cells were treated with 30 μM Zn with (U73122, orage; 2APB, light orage) or without (black) the pre-incubated 3 μM U73122 or 20 μM 2APB. (B) Quantification of the inhibitory effect of U73122 or 2APB on Zn-induced intracellular calcium increase.

Figure 2-8. Zn exhibits heterologous desensitization with muscarinic and histamine receptors. (A-B) Fura-2 loaded HSG cells were treated with 30 µM Zn and 300 µM carbacohol in order and their traces of the fluorescence ratio of F340/F380 were monitored. Pretreatment of Zn made the inhibition of intracellular Ca^{2+} level triggered with carbachol and the results are similar in reverse order. (C-D) Fura-2 loaded HSG cells were treated with 30 µM Zn and 100 µM histamine in order and their traces of the fluorescence ratio of F340/F380 were monitored. Pretreatment of Zn made the inhibition of intracellular Ca^{2+} level triggered with histamine and the results are similar in reverse order.
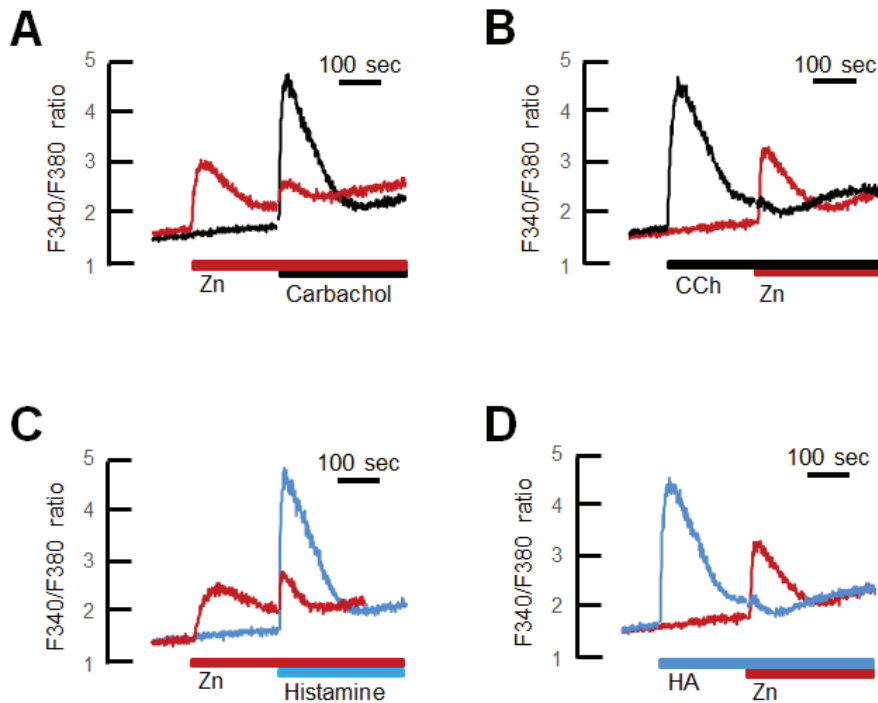
Figure 2-9. Muscarinic receptor activation exhibits heterologous desensitization with histamine receptors. (A-B) Fura-2 loaded HSG cells were treated with 300 µM carbachol and 100 µM histamine in order and their traces of the fluorescence ratio of F340/F380 were monitored. Pretreatment of Carbachol made the inhibition of intracellular Ca^{2+} level triggered with histamine and the results are similar in reverse order.
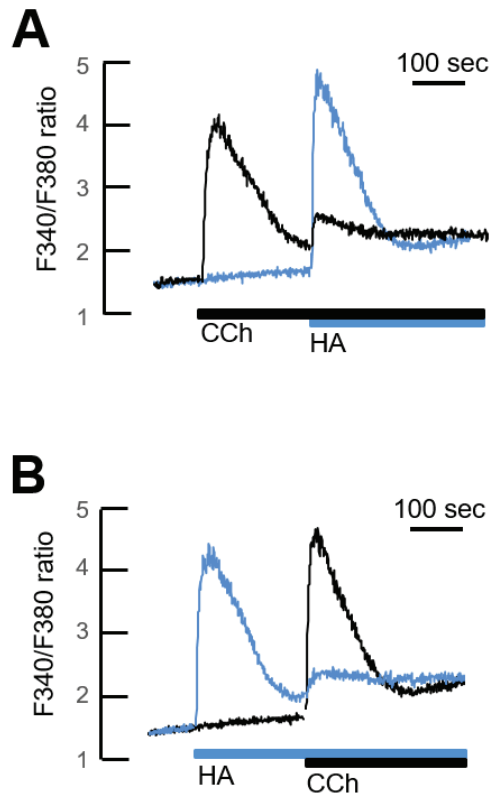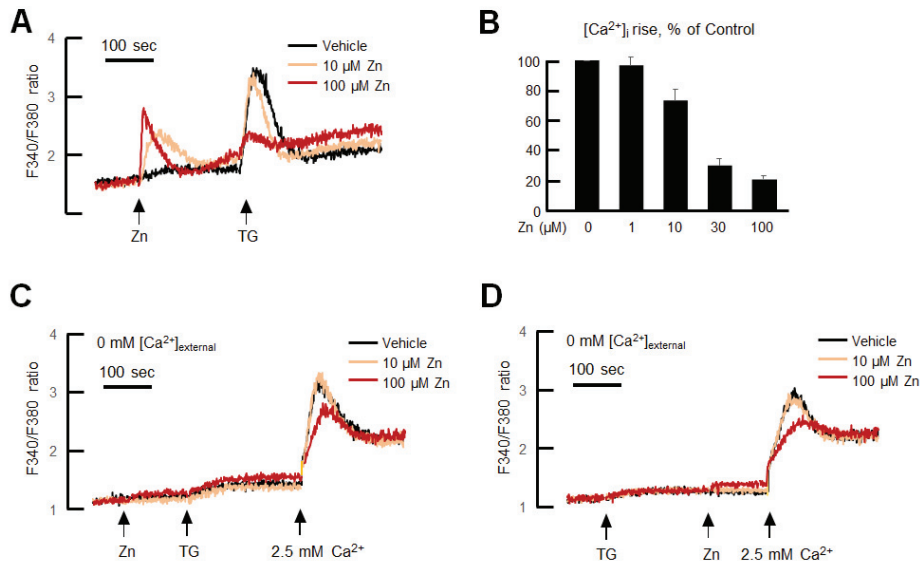
Figure 2-10. Zn inhibits thapsigargin-induced $[Ca^{2+}]_i$ rise in HSG cells. (A-B) Fura-2-loaded HSG cells were treated with 1 μM thapsigargin with or without the pre-incubated Zn at various concentrations (100 μM, red; 10 μM, pink; vehicle, black). (C-D) Fura-2-loaded HSG cells were pretreated with Zn with various concentration (100 μM, red; 10 μM, pink; vehicle, black) in the extracellular Ca^{2+}-free condition, as indicated, and then stimulated with 1 μM thapsigargin in the absence of extracellular Ca^{2+}. Ca^{2+} influx was induced by adding 2.5 mM $CaCl_2$ (Ca^{2+}) into the extracellular space. (C) (D), the order of zinc and TG was changed
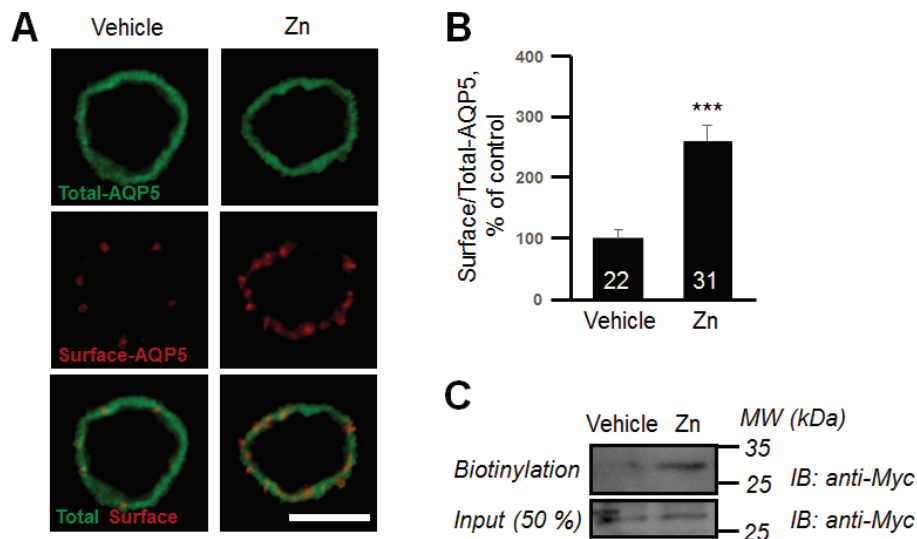
Figure 2-11. Zn^{2+} successfully increases the surface aquaporin-5 level of the plasma membrane in HSG cells. (A-C) AQP5-Myc transfected HSG cells were treated with Zn^{2+} and membrane translocation of AQP5 was confirmed. (A) Confocal images of transfected HSG cells stained with total-AQP5 (green) and surface-AQP5 (red). Scale bar: 5 µm. (B) Quantification of surface-to-total Myc-AQP5 ratio. Values are presented as percentages of vehicle. (C) HSG cells were used for steady-stated biotinylation of surface Myc tagged AQP5 channel. Input (50 %) of total lysate are shown on the bottom, and the biotinylated surface BK channels are shown above it. Each point shown is the mean ± SEM. ***$P < 0.001$, compared to vehicle control.

CHAPTER III

Chlorpromazine inhibits muscarinic and histamine receptor signaling in salivary gland cells.

3.1. Introduction

Salivary glands are exocrine glands of the oral cavity that secrete saliva and perform important functions. When saliva secretion problems occur, various oral diseases are induced (Pedersen et al., 2018). There are several factors that may reduce the saliva secretion, such as autoimmune diseases such as Sjogren's syndrome, and the death of salivary cells caused by irradiation. One of the important factors is extrinsic medicine (Proctor, 2016; Bhattarai et al., 2018). It has been known that various drugs such as antihistamine, anticholine, and diuretics have been shown to decrease saliva secretion, and their functional groups have been found in many aspects (Villa et al., 2016; Wolff et al., 2017; 2018).

Many neurological and psychiatric drugs cause xerostomia (Cockburn et al., 2017). These are clinically more important because they are prescribed chronically and cause prolonged xerostomia. One of the drugs causing severe xerostomia is chlorpromazine (Conley et al., 1998). Chlorpromazine is an antipsychotics drug mainly prescribed for schizophrenia (Rosenbloom, 2002). Since the 1950s, chlorpromazine has been widely used for the treatment of psychosis and manic syndrome. It has been prescribed for the reduction of positive symptom in schizophrenia patients including hallucination and delusion. Chlorpromazine acts mainly as a dopamine D2 receptor inhibitor, similar to other neuroleptics (Kapur and Mamo, 2003; Carpenter and Koenig, 2008). However, there is no clear molecular mechanism for how chlorpromazine inhibits secretory function in salivary glands. It is assumed that D2 receptor hypothesis is not suitable to explain xerostomia of chlorpromazine because the function of dopamine receptor is not known in salivary gland.

As I reviewed in the previous chapter, salivary secretion is precisely regulated by the action of neurotransmitters under the control of neurons, in which intracellular calcium signaling is important (Ambudkar, 2016). Significant calcium signals in salivary gland cells, which are non-excitable cells, are signaled by GPCRs. Parasympathetic modulation, the most important regulator of salivary secretion, is ultimately due to the activation of muscarinic receptors and the resulting increase in intracellular calcium (Proctor, 2016). Therefore, it is worthy to investigate the effect of chlorpromazine on the calcium regulation in salivary gland cells.

In this chapter, I have studied how chlorpromazine regulates intracellular calcium signaling in salivary glands. I found that chlorpromazine inhibits carbachol- and histamine-induced Ca^{2+} signaling, and also inhibits thapsigargin-mediated $[Ca^{2+}]_i$ increase. I would like to report that chlorpromazine inhibits SOCE as well.

3.2. Materials and Methods

Materials

Carbachol, histamine and sulfinpyrazone were purchased from Sigma (St. Louis, MO, USA). Chlorpromazine and SK&F96365 were obtained from Tocris (Bristol, UK). Thapsigargin was purchased from Alomone Labs (Jerusalem, Israel). Fura-2/acetoxymethylester (Fura-2/AM) was obtained from Molecular Probes (Eugene, OR, USA). Fetal bovine serum, modified Eagle's Medium, and penicillin/streptomycin were purchased from Gibco (Grand Island, NY, USA). Myc tagged AQP5 construct was purchased from Origene (Rockville, MD, USA).

Cell culture

HSG cells were maintained in Dulbecco's modified Eagle's medium (DMEM) supplemented with 10% heat-inactivated fetal bovine serum and 1% penicillin/streptomycin. The cell line was cultured in a humidified atmosphere of 95% air + 5% CO_2. The culture medium was changed every day, and the cell lines were subcultured every 3 day.

Measurement of saliva flow rates

To measure stimulated flow rates of saliva, total saliva of an anesthetized 10 week-old BL6 mouse was collected. Individual mice were weighed and given an i.p. injection of 10 mg /kg chlorpromazine plus 300 μg/kg pilocarpine. Saliva was collected for 10 min from the oral cavity of individual mice using a micropipette starting 1 min after injection of the secretagogue. The volume of each saliva sample was measured.

Measurement of intracellular Ca^{2+} concentrations ($[Ca^{2+}]_i$)

The fluorescent Ca^{2+} indicator, fura-2, was used to determine $[Ca^{2+}]_i$ according to previously reported methods (Choi et al., 2016). Briefly, cell suspensions were incubated in Locke's solution (154 mM NaCl, 5.6 mM KCl, 10 mM glucose, 2.2 mM $CaCl_2$, 1.2 mM $MgCl_2$, and 5 mM HEPES buffer adjusted to pH 7.4) supplemented with 3 µM fura-2/AM for 50 min at 37 ^{o}C with continuous stirring. Fluorescence ratios were monitored using 340 and 380 nm dual excitation wavelengths. The ratio of resultant intensities was detected at a 500 nm emission wavelength. Fluorescence ratios were converted into $[Ca^{2+}]_i$ as described by Grynkiewicz *et al.,*(1985). Extracellular Ca^{2+}-free solution was 200 µM EGTA-containing Ca^{2+} free Locke's solution (156.2 mM NaCl, 5.6 mM KCl, 1.2 mM $MgCl_2$, 5 mM HEPES, 10 mM glucose, adjusted to pH 7.4). Where indicated, 2.5 mM $CaCl_2$ was added to monitor subsequent Ca^{2+} influx.

Cell Transfection and Cell surface biotinylation

Cells were transfected using Lipofectamine 2000 (Invitrogen), according to the manufacturer's instructions. HSG cells were transfected with pCMV6-AQP5-Myc construct and stimulated with 100 µM Zn (30 minutes at 37 °C) in Locke's solution. To biotinylate the cell surface proteins, cells were labeled with 1.5 mg/ml sulfo-NHS-SS-biotin (Thermo Scientific, 21331) at 4 °C for 20 minutes. Following biotin labeling HSG cells were washed with respective buffer containing 100 mM glycine, and lysed with RIPA buffer. The lysates were then centrifuged at 14,000x g for 15 min at 4 °C and supernatant was collected. Protein concentrations were determined using the BCA Protein Assay Kit (Thermo Scientific, 23225) and biotinylated proteins were pulled down by incubating with NeutrAvidin agarose resins (Thermo Scientific,

29200) for overnight at 4 °C with an end to end rotation. The beads were then washed and the bound proteins were eluted by boiling in SDS dye. The eluted material was analyzed by western blotting.

Statistical analysis

Data analyses and graphical display were performed with SigmaPlot (Version 11.0, Systat Software, Germany). All displayed values represent the mean ± SEM. Significant differences between groups were determined using independent or paired Student's t-tests or Mann-Whitney U test, and multiple comparisons were performed using two-way ANOVA.

3. 3. Results

3.3.1. Chlorpromazine decreased muscarinic-induced saliva secretion.

To determine whether chlorpromazine actually affects saliva secretion, I used a mouse model to monitor the salivation. A similar amount of saliva secretion occurred ($P = 0.58$) regardless of treatment with chlorpromazine in the absence of stimulation. However, treatment with pilocarpine, a muscarnic receptor agonist used for the treatment of glaucoma, dramatically increased saliva secretion. Interestingly, chlorpromazine treatment significantly reduced secretion (Fig. 3-1). The results mean that chlorpromazine, which induces xerostomia, inhibits muscarinic signaling.

3.3.2. Chlorpromazine inhibits muscarinic and histamine-induced $[Ca^{2+}]_i$ increases in human salivary gland HSG cells.

Human salivary gland, a non-excitatory cell, is known to regulate saliva secretion through intracellular calcium regulation via several GPCRs. I used Fura-2AM loaded HSG cells to determine whether chlorpromazine affects intracellular calcium changes. Similar to Fig. 3-1, pretreatment with chlorpromazine inhibited carbachol-induced increase in intracellular calcium (Fig. 3-2A). It shows a concentration-dependent manner, with a range of 30 nM to 10 μM (Fig. 3-2B). These inhibitory effects were also found in histamine receptors as well as muscarinic receptors (Fig. 3-2C & D). Chlorpromazine inhibits histamine-induced $[Ca^{2+}]_i$ increase more strongly that the muscarinic inhibition (Fig. 3-2B, D). As a result, chlorpromazine inhibits all of the intracellular calcium increases via the muscarinic and histamine receptors, the major GPCRs of HSG cells.

3.3.3. Chlorpromazine inhibits thapsigargin-induced $[Ca^{2+}]i$ in HSG cells.

In HSG cells, it is well known that store-operated Ca^{2+} entry (SOCE) is activated by calcium depletion in intracellular stores, ER, after the activation of GPCR. After pretreatment of chlorpromazine and SOCE inhibitors in extracellular Ca^{2+} free condition, 1 μM of thapsigargin was treated to induce calcium depletion of ER, activating SOCE of cells and adding calcium. $[Ca^{2+}]_i$ was blocked by pretreatments of chlorpromazine or 1-{-[3-(4-methoxyphenyl) propoxy]- 4methoxyphenyl}-1H-imidazole hydrochloride (SK&F96365) as a SOCE inhibitor (Fig. 3-3). It was also confirmed that the inhibitory effect of chlorpromazine on this SOCE-mediated $[Ca^{2+}]_i$ acts in a concentration-dependent manner (Fig. 3-4). As a result, chlorpromazine inhibits intracellular calcium through SOCE.

3.3.4. Chlorpromazine inhibits both Ca^{2+} release from ER and Ca^{2+} influx via SOCE in HSG cells.

I have identified intracellular Ca^{2+} release and Ca^{2+} influx by chlorpromazine in order to refine at what stage chlorpromazine-mediated inhibition of muscarinic-induced intracellular calcium increases. After pretreatment of chlorpromazine in extracellular Ca^{2+} free condition, carbachol was treated to activate muscarinic receptors and calcium was added. As a result, the Ca^{2+} release from ER activated by muscarnic signal was inhibited in 30 nM chlorpromazine and completely suppressed in 1 μM chlorpromazine (Fig. 3-5A-C). On the other hand, the extracellular Ca^{2+} influx through SOCE was inhibited at a relatively higher level compared to Ca^{2+} release (Fig. 3-5). This indicates that chlorpromazine inhibits muscarinic receptor-mediated calcium signal through various inhibitory sites such as ER and SOCE.

3.3.5. *Chlorpromazine inhibits charbachol- and histamine-induced aquaporin-5 translocation to plasma membrane.*

To test whether chlorpromazine inhibits salivation *in vitro* model, I tried to test the effect of chlorpromazine on the carbachol- or histamine-induced aquaporin-5 translocation with biotinylation experiments of surface proteins. Notably, chlorpromazine successfully inhibited the both carbachol- and histamine-induced increase in biotinylated aquaporin-5 level in the plasma membrane (Fig. 3-6), suggesting the mechanism for the xerogenic effect of chlorpromazine.

3.4. Discussion

In this chapter, I found that chlorpromazine inhibits the increase of intracellular calcium by muscarinic receptor and histamine receptor, not dopaminergic D2 receptor in salivary gland cells. Also I found that chlorpromazine inhibited thapsigargin-induced store-operated Ca^{2+} entry and Ca^{2+} release from ER. These results suggest that chlorpromazine has various inhibitory action points over at least ER and SOCE.

Chlorpromazine has been known to have a variety of target sites in addition to dopaminergic receptors due to its tricyclic chemical structure. Chlorpromazine has been known to suppress many other channels and receptors such as hERG in addition to the dopamine receptor (Arias, 1997; Welch and Chue, 2000). Chlorpromazine has also been reported to inhibit SOCE in PC12 (Choi et al., 2001). Recently, however, I have found that the SOCE of PC12 is different from the SOCE of other non-excitable cells. Therefore, it is important to investigate the SOCE characteristics of salivary gland cells and how chlorpromazine controls salivary SOCE.

Recently, SOCE is one of the most important mechanisms in GPCR-Ca^{2+} signaling. It remains to be seen how they function. Orai1 KO has several defects including immunodeficiency according to the Feske group's pioneering works (Feske, 2007). Since SOCE is a key signaling mechanism of salivary GPCRs including muscarinic receptors, it is very important as a modulator of salivary function. I believe that my study will be helpful for understanding the mechanism of xerostomia in the future because there are many substances that show modulating effect on SOCE.
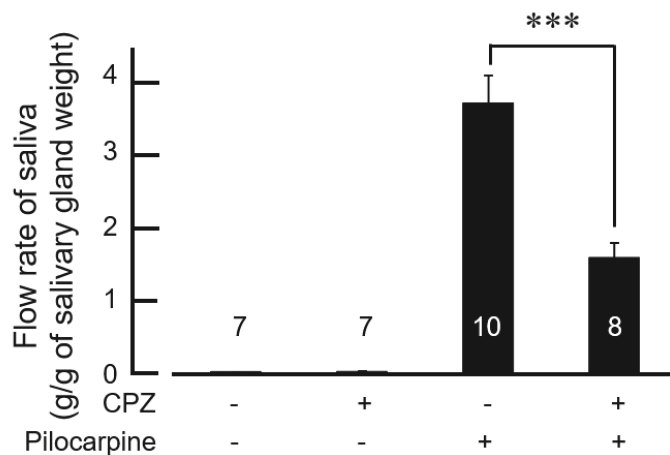
Figure 3-1. Decreased muscarinic-induced saliva flow by chlorpromazine. Total saliva of an anesthetized 10 weeks old BL6 mouse was collected. Secretion of saliva was stimulated by intraperitoneal injection of 10 mg /kg chlorpromazine plus 300 μg/kg pilocarpine. All data shown are mean ± SEM (by independent Student's t-test).
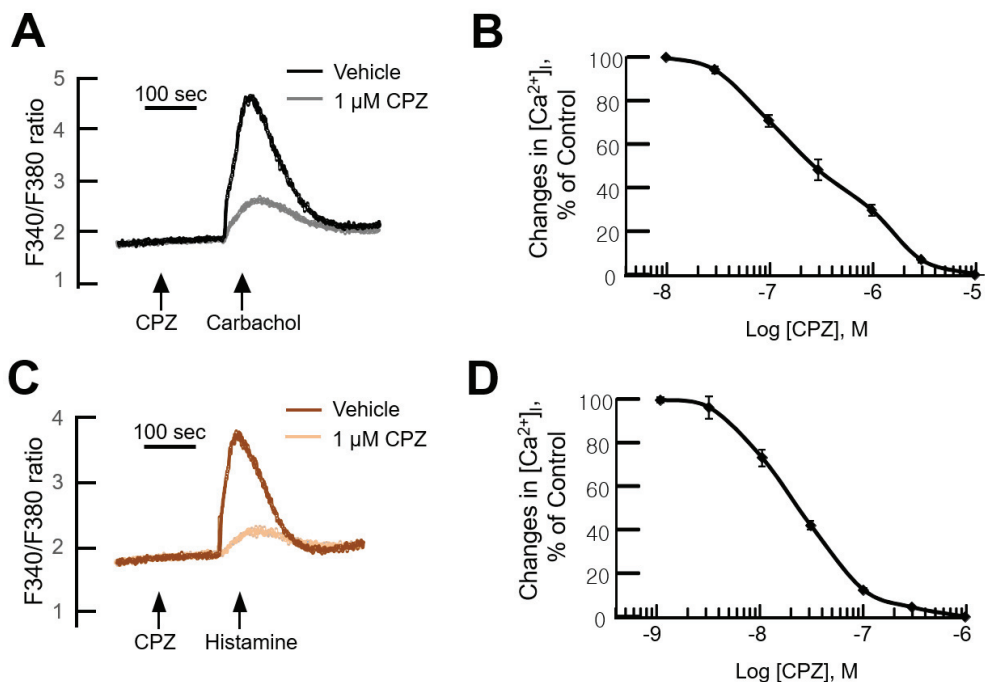
Figure 3-2. Chlorpromazine inhibits carbachol & histamine-mediated increases in intracellular calcium levels by concentration-dependent manners. (A) Fura-2-loaded HSG cells were pre-incubated with chlorpromazine (1 μM, light gray; vehicle, black), stimulated with 300 μM carbachol, and the change in fluorescence ratio of F340 / F380 was monitored at $[Ca^{2+}]_i$ level. (B) Cells were pre-incubated with chlorpromazine with the indicated concentraions, and the inhibition of 300 μM carbacohol-induced increase in Ca^{2+} was monitored. (C) Fura-2-loaded HSG cells were pre-incubated with chlorpromazine (1 μM, light brown; vehicle, brown), stimulated with 100 μM histamine, and the change in fluorescence ratio of F340 / F380 was monitored at $[Ca^{2+}]_i$ level. (D) Cells were pre-incubated with chlorpromazine with the indicated concentraions, and the inhibition of 100 μM histamine-induced increase in Ca^{2+} was monitored.
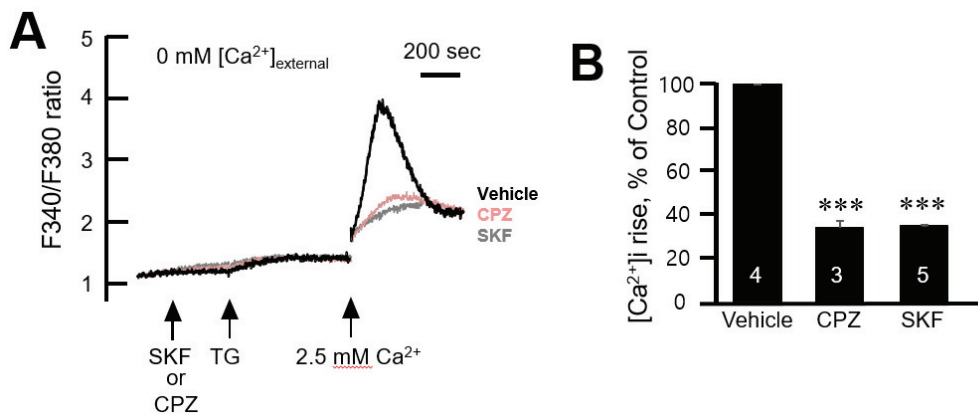
Figure 3-3. Chlorpromazine inhibits thapsigargin-induced $[Ca^{2+}]_i$ rise in HSG cells. (A) Fura-2-loaded HSG cells were pretreated with inhibitors in the extracellular Ca^{2+}-free condition, as indicated, and then stimulated with 1 μM thapsigargin in the absence of extracellular Ca^{2+}. Ca^{2+} influx was induced by adding 2.5 mM $CaCl_2$ (Ca^{2+}) into the extracellular space: vehicle (black), 30 μM chlorpromazine (pink) and 20 μM SKF (light gray). Inhibitor and chlorpromazine were pretreated 210 s prior to thapsigargin treatment. (B) Peak levels of thapsigargin-induced $[Ca^{2+}]_i$ influx after $CaCl_2$ treatment were quantitatively analyzed and depicted as % of the thapsigargin-induced $[Ca^{2+}]$ rise without inhibitor treatment. Number of experiments is depicted in bar graph. Each point shown is the mean ± SEM. ***P < 0.001, compared to vehicle control

63
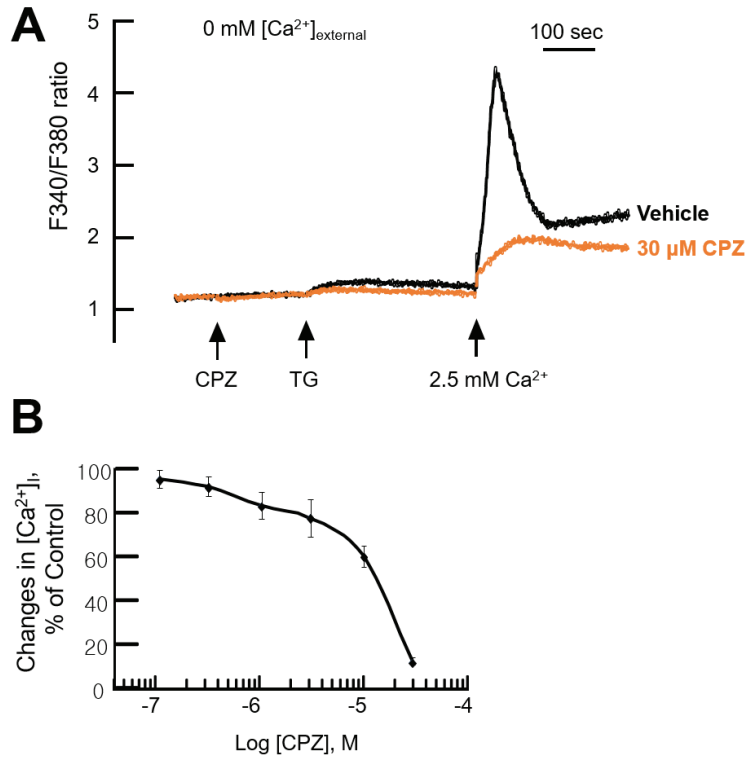
Figure 3-4. Chlorpromazine inhibits thapsigargin-induced $[Ca^{2+}]_i$ rise in HSG cells by concentration-dependent manners. (A) Fura-2-loaded HSG cells were pre-incubated with chlorpromazine (30 μM, orage; vehicle, black), stimulated with 1 μM thapsigargin, and the change in fluorescence ratio of F340 / F380 was monitored at $[Ca^{2+}]_i$ level. (B) Cells were pre-incubated with chlorpromazine with the indicated concentraions, and the inhibition of 1 μM thapsigargin-induced increase in Ca^{2+} was monitored.
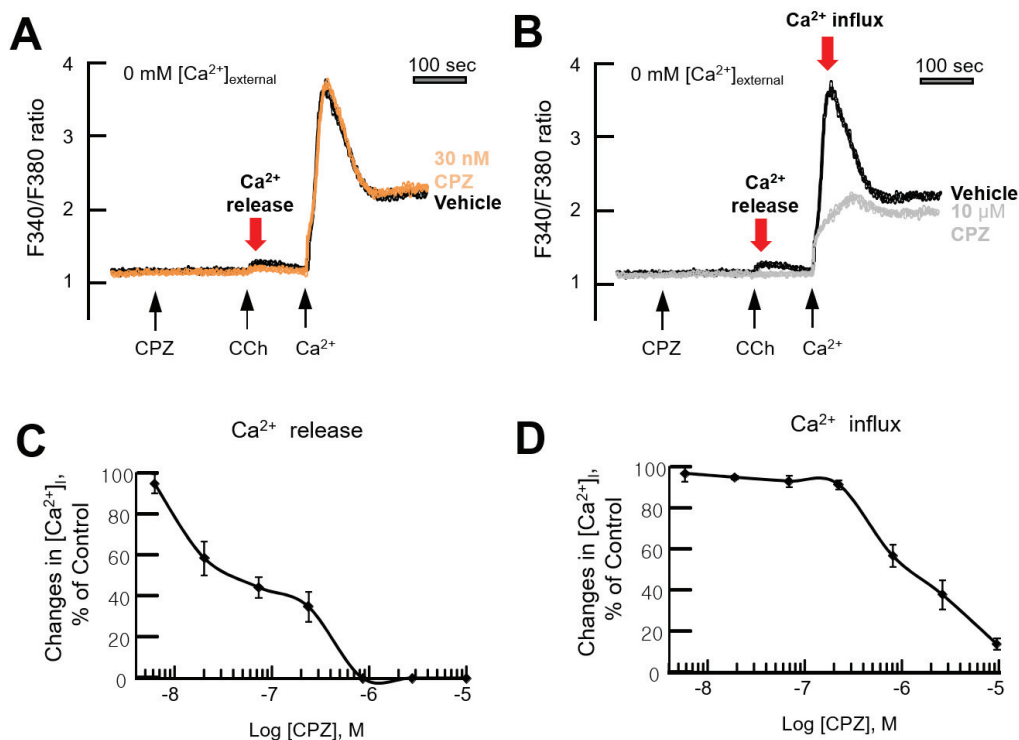
Figure 3-5. Inhibition of muscarinic-induced intracellular calcium increase by chlorpromazine is mediated through Ca^{2+} release in ER and Ca^{2+} influx through SOCE. (A-B) Fura-2-loaded HSG cells were pre-incubated with chlorpromazine (30 nM, orage; vehicle, black in A; 10 µM, light gray; vehicle, black in B), stimulated with 300 μM carbachol, and the change in fluorescence ratio of F340 / F380 was monitored at $[Ca^{2+}]_i$ level. (C-D) In the extracellular Ca^{2+}-free condition, cells were preincubated with chlorpromazine at indicated concentrations and the degree of inhibition of carbachol-induced $[Ca^{2+}]_i$ by chlorphromazine was monitored in both Ca^{2+} release (C) and Ca^{2+} influx (D).
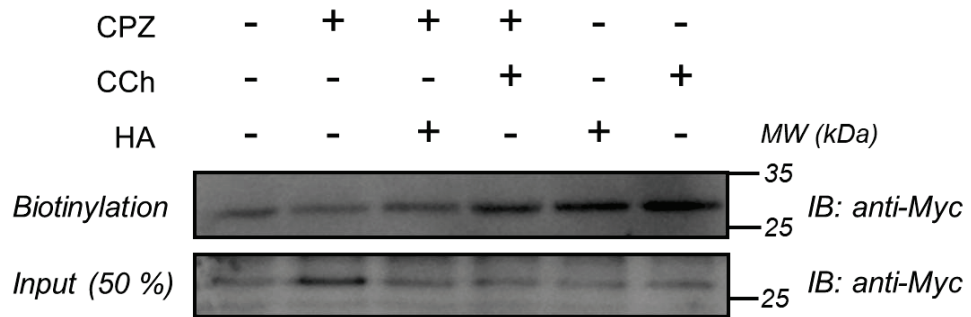
Figure 3-6. Chlorpromazine inhibits carbachol- and histamine-induced aquaporin-5 translocation in HSG cells. AQP5-Myc transfected HSG cells were treated with chlorpromazine, carbachol and histamine, and membrane translocation of AQP5 was confirmed. Input (50 %) of total lysate are shown on the bottom, and the biotinylated surface AQP5 channels are shown above it.

CHAPTER IV

Ca^{2+}-activated K^+ channel (BK)

& its modulator, CRBN

4.1. Introduction

Calcium is a ubiquitous intracellular signal that regulates numerous cell processes such as gene transcription, cell motility, and muscle contraction. An increase in intracellular calcium regulates the activity of ion channels present in the cell membrane to perform various processes. The BK channel, Ca^{2+} activated K channel, which is downstream of cytosolic Ca^{2+} signaling, is known to be expressed in various tissues including neurons, smooth muscle, skeletal muscle and endocrine cells.

The BK channel is a large conductance Ca^{2+} activated K channel consisting of four α subunits that constitute the pore and β subunit that is important for ER retention. The BK channel moves K^+ out of the cell, thereby accelerating the repolarization of the action potential (AP) and controlling neuronal excitability. They are also known to inhibit neurotransmitter release by reducing AP duration. Therefore, it is known that overexpression of α subunit that constitutes a pore, or deletion of a β subunit that plays an ER retention role, increases channel activity and ultimately induces epilepsy or neurological disease. Therefore, regulation of surface expression of BK channels in cells is a very important issue.

Cereblon (CRBN) is a key factor that regulates the surface level of this BK channel, and binding with BK induces ER retention. Therefore, CRBN decreases the surface expression of the BK channel. CRBN gene was located on chromosome 3 (3p26.3) exon 11 and highly conserved from plant to man. A nonsense (c.1274CT) or missense (c.1171TC) mutation in the CRBN gene is suspected to cause intellectual disability (ID) in humans (Higgins et al., 2004, 2008; Sheereen et al., 2017). Deletion or microduplication of 3p26.3

including CRBN also results in cognitive and behavioral impairment (Dijkhuizen et al., 2006; Papuc et al., 2015). My lab has identified physiological defects in the CRBN that regulates the surface expression level of the BK channel. As a result, the excitatory release probability decreased in the hippocampus of *Crbn* KO mice, confirming that this was due to the hyperactivity of BK channels.

However, despite the fact that the study of CRBN has evolved from its identification as a mild intellectual disability causal factor, the cellular and molecular mechanisms of cognitive impairment caused by CRBN mutations remain unclear. In fact, my lab had investigated the function of CRBN using CRBN KO animal model, but it is unclear whether the CRBN KO condition (i.e. null mutant) has the same phenotype as the CRBN mutation in the patients (i.e. nonsense mutant, R419X).

I confirmed whether the decrease of the release probability observed in the CNS was also observed in the PNS, and whether CRBN R419X mutants observed in the ID patients and CRBN null mutants showed the same phenotype. To do this, I used the *Drosophila* NMJ system, which represents excitatory synapse in the PNS area.

4.2. Materials and Methods

Experimental animals

Drosophila strains were raised on a standard yeast, sugar, and agar medium at 25°C. The WT strain was w[1118] unless otherwise noted. *CRBN[ex1], UAS-Myc-CRBN* and *UAS-Myc-CRBNG552X* were obtained from Dr. Jongkyeong Chung in National Creative Research Initiatives Center for Energy Homeostasis Regulation (Institute of Molecular Biology and Genetics and School of Biological Sciences, Seoul National University). *Df(3R)BSC621* (a deficiency uncovering the CRBN locus, #25696) and *C155-GAL4* (pan-neuronal driver, #458) were obtained from Bloomington Stock Center.

All mice were housed in an animal facility with a specific pathogen-free barrier under a 12 h light/dark cycle. Mice were allowed access to food and water *ad libitum*. Wild-type (WT) and *Crbn* KO male mice (Lee et al., 2013) from the C57BL/6 background were used. All experiments were approved by the Institutional Animal Care and Use Committee at Seoul National University and the Gwangju Institute of Science and Technology Animal Care and Use Committee.

Electrophysiology

Drosophila NMJ recordings Two-electrode voltage-clamp (TEVC) recordings of wandering third-instar female *Drosophila* larvae NMJ were obtained from ventral longitudinal muscle 6 in segment A3–A4 at room temperature as described previously with modifications (Karr et al., 2009). All dissections and recording were performed in HL3.1 saline containing the following (in mM): 70 NaCl, 5 KCl, 4 MgCl$_2$, 5 trehalose, 115 sucrose, and 5 HEPES (Feng et al., 2004). Larval dissection was performed in Ca^{2+}-free saline to minimize

muscle contraction. TEVC recording was performed with 2 mM Ca^{2+}. Recording electrodes were filled with 3 M KCl, which had a resistance of 10–15 MΩ. Recordings were made from cells with an initial resting membrane potential between -60 and -70 mV at a holding potential of -70 mV with a Gene clamp 500 amplifier (Molecular Devices). The cut segmental nerve was stimulated with a glass suction electrode at a suprathreshold level (5 mA) for 0.2 ms. Signals were filtered at 10,000 Hz, acquired with Axoscope version 10.2 software (Molecular Devices), and analyzed with Clampfit version 10.2 software (Molecular Devices). EPSC amplitudes were measured from peak to the baseline immediately before EPSC onset.

Whole-cell recordings. Cells were transferred to a recording chamber where they were perfused continuously with ACSF gassed with 95% O_2/5% CO_2 at a flow rate of 2 ml/min. Cells were equilibrated for 5 min before the recordings and all of the experiments were performed at 23–25°C. Recordings were obtained using Axon Digidata 1550B (Axon Instruments) and patch clamp EPC8 (HEKA). Patch pipettes (4–6 MΩ) were filled with the following (in mM): 135 K-gluconate, 8 NaCl, 10 HEPES, 2 ATP-Na, and 0.2 GTP-Na (for calcium-activated potassium current experiments) (Aoki and Baraban, 2000) at a pH of 7.4 and 280–290 mOsm.

Primary neuronal culture and transfection

Primary hippocampal neurons were isolated from the early postnatal day 0 (P0) to P1 WT and *Crbn* KO mice brains. Hippocampi were digested with trypsin (Invitrogen, 15090) and DNase (Sigma-Aldrich, DN25). Dissociated neurons were plated on poly-L-lysine coated coverslips at 3 X 10^5 cells per well. Neurons were maintained in neurobasal-A medium (Invitrogen, 10888-022) supplemented with B-27 (Invitrogen, 17504044), GlutaMAX-I

(Invitrogen, 35050-061), and 1 % penicillin/streptomycin in a humidified 5% CO_2 incubator at 37°C. Two days after plating, 2.5 μ M cytosine arabinoside was added to inhibit the non-neuronal cells. Twice a week there after, half of the medium was exchanged with fresh maintenance medium. Cultured hippocampal neurons were transfected with DNA constructs (human wild CRBN and R419X) at 7 d *in vitro* (DIV7) using calcium phosphate. Experiments were performed at DIV9-14.

Western blot analysis

Larval brain and VNC were homogenized in 1 × SDS sample buffer, subjected to SDS-PAGE. Blots were blocked in 5% skim milk/TBST (TBS, 0.2% Tween-20) and incubated with primary antibodies in 5% skim milk/TBST overnight at 4 °C. After several washes in TBST, blots were incubated for 1 h with HRP-conjugated secondary antibodies in 5% skim milk/TBST. Blots were washed several times with TBST and visualized with SuperSignal West Pico CL substrate (Pierce). Antibodies were used at the following dilutions: anti-Myc (1:1000), anti-β-actin (1:1000), and HRP-conjugated secondary antibodies (1:5000, Jackson Laboratories).

Immunohistochemistry

Wandering third instar larvae were dissected in Ca^{2+}-free HL3 saline (5 mM HEPES, 70 mM NaCl, 5 mM KCl, 20 mM $MgCl_2$, 10 mM $NaHCO_3$, 5 mM trehalose, 115 mM sucrose [pH 7.2]) (Stewart et al., 1994) and fixed in 4% formaldehyde/PBS for 30 min. Fixed larvae were washed in PBT (PBS, 0.1% Triton X-100), blocked with 5% BSA/PBT for 1 h, and incubated with primary antibodies at 4 °C overnight. After several washes with PBT, dissections were incubated with secondary antibodies for 1 h at room

temperature. Fluorescence images were collected under a Confocal Laser Scanning Microsope (Carl Zeiss, LSM700).

Statistical analysis

Data analyses and graphical display were performed with SigmaPlot version 11.0 software (Systat Software). All displayed values represent the mean SEM. Significant differences between groups were determined using independent or paired Student's t tests or Mann– Whitney U test and multiple comparisons were performed using two-way ANOVA.

4.3. Results

4.3.1. Drosophila Crbn loss-of-function mutants show decreased probability of neurotransmission release not rescued by the overexpression of the CRBN G552X mutant.

Crbn KO mice and *Drosophila CRBX^ex1* mutant showed decreased neurotransmitter Pr in excitatory synapses without detectable structural phenotypes. However, phenotypes observed in knock-out mutants are not synonymous with R419X observed in human mild intellectual disability patients. I performed a rescue experiment to confirm that CRBN R419X and CRBN null mutants had the same action. First, I performed the rescue experiments by the reintroduction of CRBN G522X, a human R419X mimic form (Fig. 4-1), using the *Drosophila* NMJ system, a glutamatergic synapse. Using a pan-neuronal *C155-GAL4* driver and *UAS-Crbn* lines, I specifically overexpressed WT CRBN in neurons with a *CRBN^ex1/Df* background (*C155-GAL4/+; UAS-Myc-CRBN/+; CRBN^ex1/Df*) and tested presynaptic release phenotypes. The overexpression of not only WT CRBN, but also the *Drosophila* CRBN G552X mutant did not affect the amplitudes of mEJCs (Fig. 4-2A, B; amplitude: $F_{(2,34)} = 1.056$, $p = 0.359$) or eEJCs (Fig. 4-3; amplitude: $F_{(2,34)} = 0.767$, $p = 0.473$) but mEJC frequency in the overexpression of CRBN G552X mutant was decreased (Fig. 4-2C; frequency: $F_{(2,34)} = 4.264$, $p = 0.022$). However, the overexpression of WT CRBN successfully rescued PPR (Fig. 4-4; ISI at 10 ms: $F_{(2,34)} = 6.637$, $p = 0.004$; ISI at 25 ms: $F_{(2,34)} = 4.055$, $p = 0.026$; ISI at 50 ms: $F_{(2,34)} = 2.474$, $p = 0.099$; ISI at 100 ms: $F_{(2,33)} = 0.493$, $p = 0.614$), and 20-pulse train stimulation induced STP (Fig.4-5; $p < 0.001$ at the fifth stimulus, $p < 0.01$ at the sixth, seventh,

and ninth stimulus, $p < 0.05$ at the second, fourth, and 11th stimulus, $p > 0.05$ at the third, eighth, 10th, and $12^{th} \sim 15^{th}$ stimulus) in $CRBN^{ex1}/Df$ mutants to the levels seen in *C155-GAL4* control flies. These rescue effects were not found in flies overexpressing the *Drosophila* CRBN G552X mutant, which mimics the human CRBN R419X pathogenic mutant (Fig. 4-4, 4-5). Together, these results strongly suggest that the presynaptic functions of CRBN are highly conserved from CNS to PNS and that presynaptic defects are caused not only by lack of *Crbn* expression, but also by the CRBN nonsense mutation that is observed in human mild intellectual disability patients (Higgins et al., 2004, 2008).

4.3.2. Human mutant form of Crbn, R419X, results in a relatively small decreased in the BK channel activity.

There is a previous report in which CRBN decreases surface expression level of BK channel by inducing ER retention (Liu et al., 2014). In addition, my lab found that a Pr decrease in *Crbn* KO mice might be due to BK channel hyperactivity by calcium-activated potassium currents ($I_{K(Ca)}$). I tested the synaptic effects of the intellectual disability related human mutant form of CRBN, R419X. For this purpose, cultured hippocampal neurons from *Crbn* KO were transfected by R419X mutant CRBN or WT CRBN and then I measured BK channel activity, $I_{K(Ca)}$, by applying brief depolarization from the holding potential (- 50 mV) under a TTX-including external solution (Aoki and Baraban, 2000). The BK channel activity of *Crbn* KO neurons with WT CRBN expression was significantly lower than that of the untransfected control neurons from *Crbn* KO mice, whereas *Crbn* KO neurons with R419X mutant CRBN expression showed a relatively small decrease in BK channel activity (Fig. 4-7; WT rescue, $t_{(18)} = 4.215$, $p < 0.001$;

R419X rescue, $t_{(19)}$ = 0.869, p = 0.396). This suggests that increased BK channel activity in *Crbn* KO neurons was reduced by WT CRBN expression, but not by R419X mutant CRBN expression.

4.3.3. *CRBN G552X, a point mutation in CRBN, has a targeting effect.*

I confirmed that Pr reduction and BK channel hyperactivity were not rescued, despite reintroduction of R419X (or G552X in *Drosophila*) in the CRBN loss-of-function mutants. To find out why R419X does not have rescue activity, I checked the targeting effect. I have confirmed CRBN expression in *Drosophila* CNS and PNS. When CRBN was presynaptically expressed, it was largely observed in brain and partially observed in ventral nerve cord (VNC) but not in NMJ (Fig 4-6A, B). However, when CRBN G552X was expressed in the same manner, CRBN 552X was observed to be expressed in VNC and axon terminal, unlike CRBN WT, but not in brain (Fig 4-6A, B). This means that the G552X point mutation shows a targeting effect. The western blot experiments confirmed that this point mutation did not affect the protein synthesis of CRBN (Fig 4-6C).

4.4. Discussion

One of the concerns regarding experiments conducted with conventional or conditional *Crbn* KO mice is whether the complete genetic deletion of the gene encoding CRBN in *Crbn* KO mice is a valid model of CRBN-associated intellectual disability in human patients. To address this question, I applied two approaches. First I used a *Drosophila* model with neuron-specific CRBN overexpression in *Crbn* KO flies using both WT and G552X mutant CRBN. *Drosophila* CRBN G552X mutation mimics the human CRBN R419X mutation, which causes mild intellectual disability. I confirmed that the defects were rescued by reintroduction of WT CRBN into *Crbn* KO flies, but not by reintroduction of the G552X mutant CRBN. I also used cultured hippocampal neurons from *Crbn* KO mice expressing human WT or R419X mutant CRBN to demonstrate that the reduced Pr in *Crbn* KO neurons is restored by reintroduction of WT CRBN, but not by R419X mutant CRBN. These results suggest that presynaptic Pr decrease can be induced by either complete loss of CRBN expression or CRBN mutation (i.e., R419X in humans and G552X in *Drosophila*).

These results confirm again that CRBN acts on the downstream of Ca^{2+} signaling, Ca^{2+}-activated K^+ channel, to regulate presynaptic neurotransmitter release, and contributes to understanding how CRBN mutation in human patients causes intellectual disability.
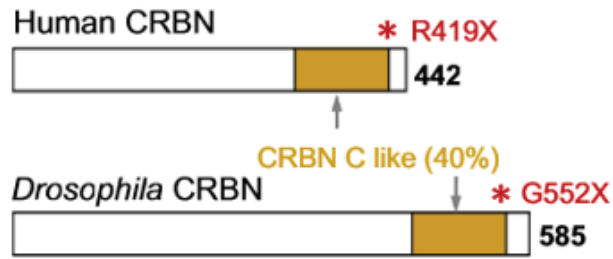
Figure 4-1. Domain structures of human CRBN and its *Drosophila* ortholog with percentage identity between their corresponding domains. CRBN C-like domain is shown in dark yellow. The single asterisks denote substitution mutations of CRBN used in this study.
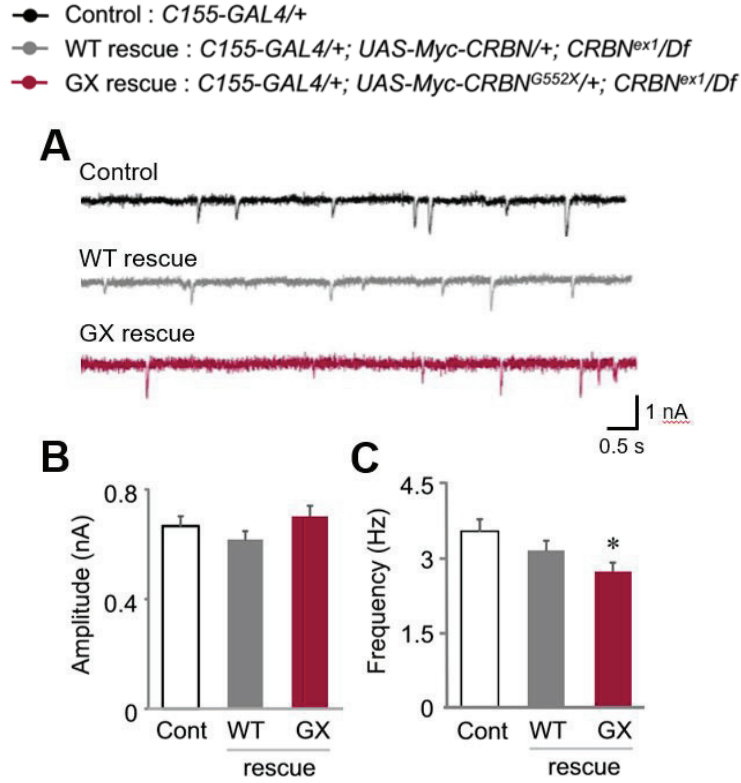
Figure 4-2. The overexpression of not only WT, but also the *Drosophila* CRBN G552X mutant did not affect the amplitudes of mEJCs. **(A)** Representative traces of spontaneous mEJCs in the following genotypes: *C155-GAL4/+* (control), *C155-GAL4/+; UAS-Myc-CRBN WT/+; CRBN^{ex1}/Df* (CRBN WT rescue) and *C155-GAL4/+; UAS-Myc-CRBN G552X/+; CRBN^{ex1}/Df* (CRBN GX rescue). (B-C) Mean amplitude and frequency of spontaneous mEJCs are shown. N =11 control; n = 8 CRBN-WT rescue; n = 18 CRBN-GX rescue. All data shown are mean SEM. ***p ＜ 0.001; **p ＜ 0.01; *p ＜ 0.05. n.s., Not significant by independent Student's t test.
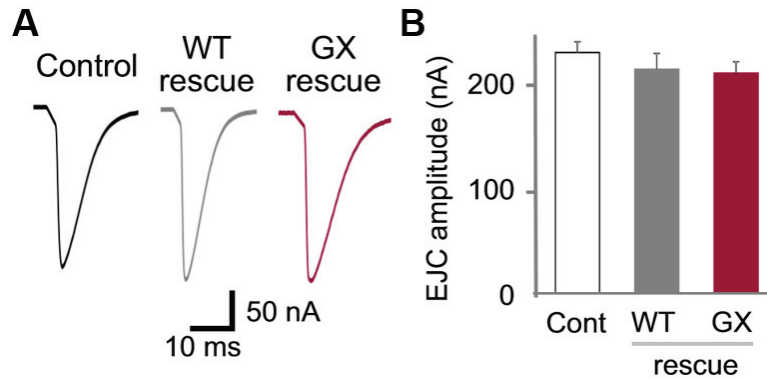
.

Figure 4-3. The overexpression of not only WT, but also the *Drosophila* CRBN G552X mutant did not affect the amplitudes of eEJCs. **(A-B)** Representative eEJC traces and mean amplitude of eEJCs in CRBN rescue animals. N = 11 control; n = 8 CRBN-WT rescue; n = 18 CRBN-GX rescue. All data shown are mean SEM.
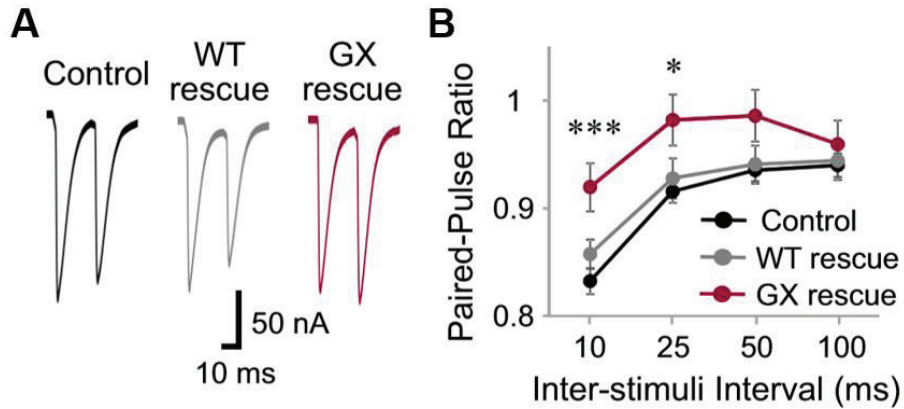
Figure 4-4. Overexpression of CRBN WT rescued the increased PPR (10 and 25 ms ISI) at *Crbn* mutant synapses but CRBN GX did not. **(A-B)** Representative traces and PPR is plotted against indicated ISIs. N = 11 control; n = 8 CRBN-WT rescue; n = 18 CRBN-GX rescue. All data shown are mean SEM. ***p < 0.001; **p < 0.01; *p < 0.05. n.s., Not significant by independent Student's t test.

Figure 4-5. 20-pulse train stimulation-induced STP at *Crbn* mutant synapses is rescued by presynaptic CRBN-WT expression but not by CRBN-GX. **(A-B)** Representative traces and the amplitudes of eEJCs are plotted against stimulus number. N = 10 control; n = 8 CRBN-WT rescue; n = 15 CRBN-GX rescue. All data shown are mean SEM. ***p < 0.001; **p < 0.01; *p < 0.05. n.s., Not significant by independent Student's t test.
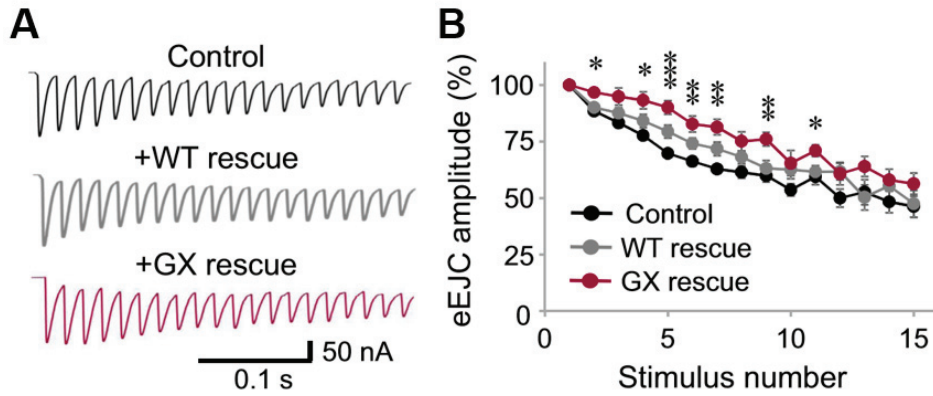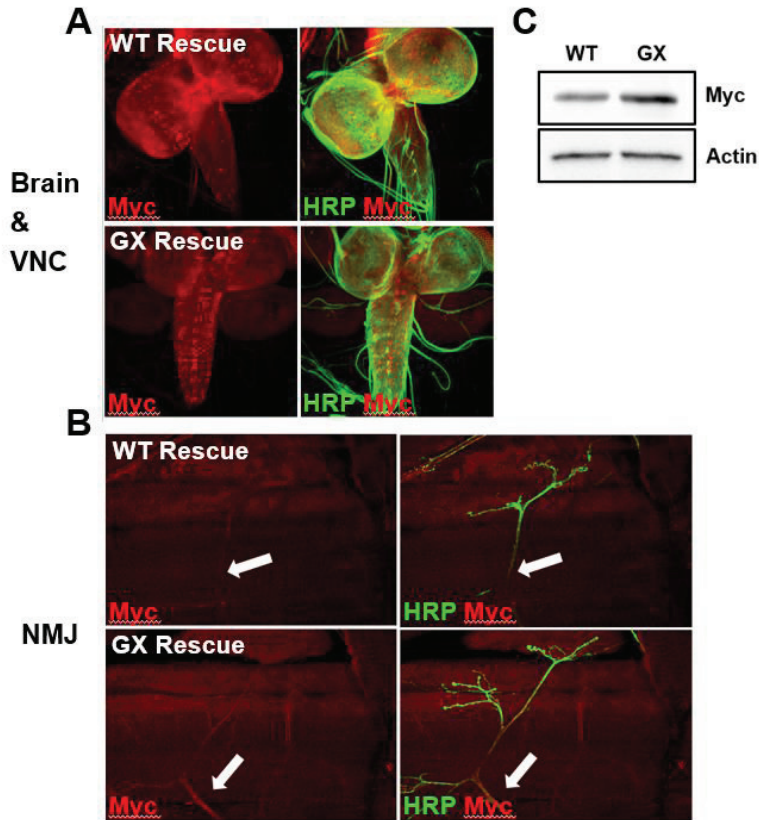
Figure 4-6. CRBN G552X, a point mutation in CRBN, has a targeting effect. **(A-B)** Confocal images of the CNS (A) and PNS (B) dissected out of wild-type third instar larvae double stained with anti-Myc (red) and anti-HRP (green). **(C)** Western blot of brain extracts of third instar WT rescue and GX rescue larvae probed with anti-Myc and reprobed with anti-β-actin.
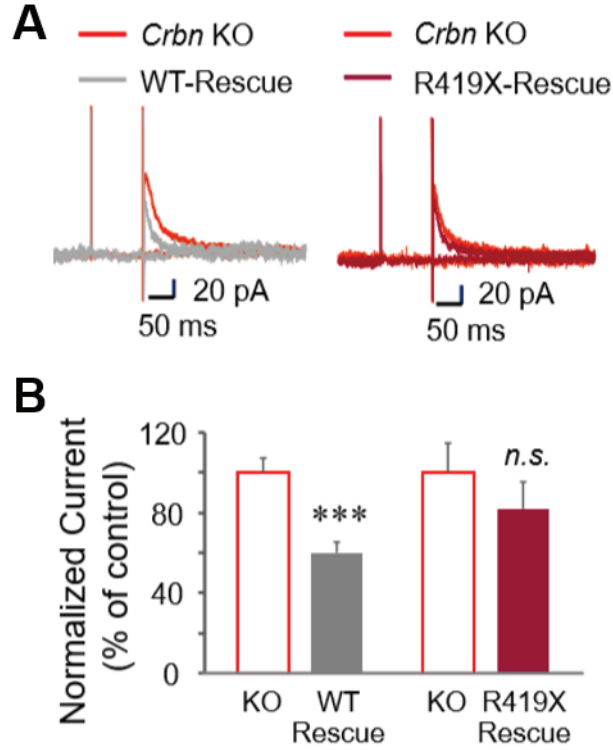
Figure 4-7. *Crbn* KO neurons with human R419X CRBN expression showed a relatively small decreased in the BK channel activity. **(A-B)** Representative $I_{K(Ca)}$ traces in untransfected (red) and transfected (grey in WT rescue; pink in R419X rescue) hippocampal neurons cultured from *Crbn* KO mice. Overexpression of CRBN WT reduced the increased $I_{K(Ca)}$ in hippocampal cultured neurons in *Crbn* KO mice but overexpression of CRBN R419X did not. n = 11 untransfected *Crbn* KO cells; n = 9 WT CRBN transfected *Crbn* KO cells (WT-Rescue); n = 11 untransfected Crbn KO cells; n = 10 R419X CRBN transfected *Crbn* KO cells (R419X-Rescue).

Conclusion

Chapter I.

Characterization of SOCE in non-excitable cells including salivary gland cells

- In most non-excitable cells, SOCE shares the Gd^{3+} dependent Orai1 mechanism
- HSG, a non-excitatory cell, is similar to PC12, an excitatory cell, and is independent of Orai1.
- TrpC dominant action in salivary gland

	2APB	SKF	Gd^{3+}	ML-9
PC12	++	++	-	+
HEK293	++	++	++	++
HL-60	++	++	+	++
Jurkat-T	++	++	+	++
HSG	++	++	-	++

Figure 1. Summary of inhibitor sensitivity in various cells.

.

Chapter II.

Zn-mediated Ca^{2+} signaling & aquaporin-5 translocation in HSG cells

- ZnR/GPR39 exists in HSG cells.
- Salivary ZnR/GPR39 is independent from Muscarinic/Histamine receptors.
- ZnR/GPR39 triggers translocation of aquaporin-5.
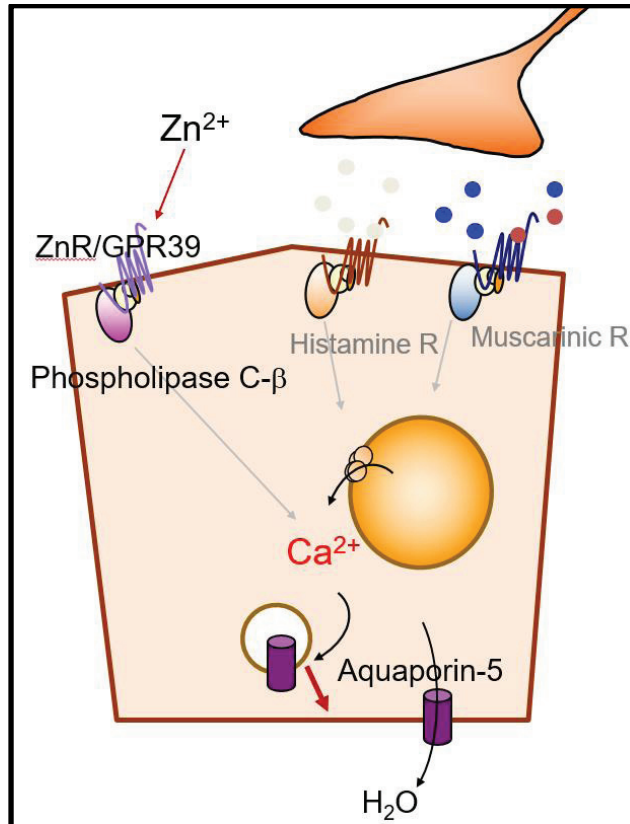- Zn may induce salivary secretion.

Figure 2. Schematic model of Zn-mediated Ca^{2+} signaling and aquaporin-5 translocation in HSG cells.

Chapter III.

Xerogenic antidepressant chlorpromazine inhibits salivary signaling

- In salivary gland cells, inhibition of Ca^{2+} signaling by chlorpromazine acts at various inhibitory sites.

    - Muscarinic Receptor - induced Ca^{2+} signaling

    - Histamine Receptor - induced Ca^{2+} signaling

    - Ca^{2+} release from ER

    - Ca^{2+} influx from SOCE

- Potent xerogenic effect due to synergistic inhibition in salivary glands.
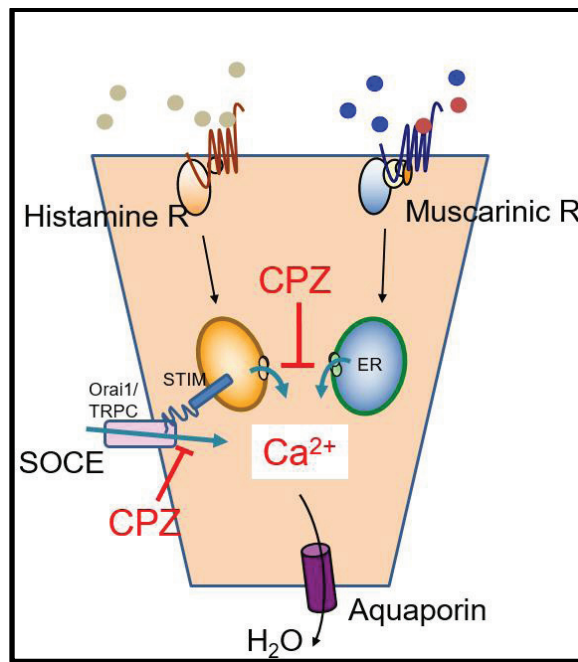
Figure 3. Schematic model of the inhibition of salivary Ca^{2+} signaling by chlorpromazine, xerogenic antidepressant.

Chapter IV.

Ca^{2+}-activated K^+ channel (BK) & its modulator, CRBN

- Similar to the CNS, the loss of CRBN in the neuromuscular junction, the PNS, affects presynaptic neurotransmitter release function via altered BK_{Ca} channel activity.

- R419X in the ID patient acts almost like a null mutant.

Figure 4. Schematic model of the relationship between CRBN and BK_{Ca}.

.

Summary

Neuronal regulation of peripheral organs mediated by calcium signaling

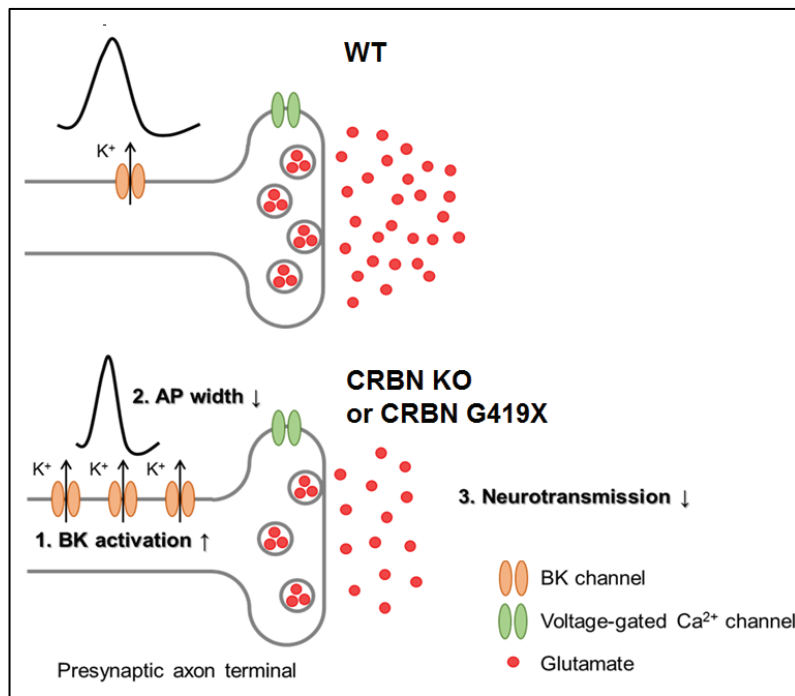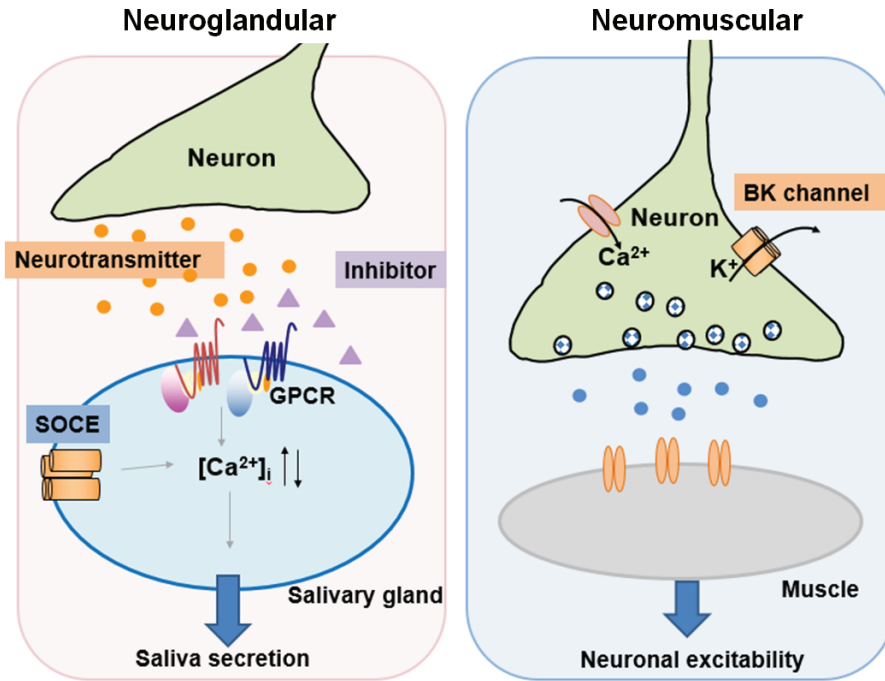**Figure 5**. Schematic model of neuronal control of peripheral functions.

REFERENCES

Ambudkar IS, de Souza LB, Ong HL. TRPC1, Orai1, and STIM1 in SOCE: Friends in tight spaces. Cell Calcium. 2017 May;63:33-39. doi: 10.1016/j.ceca.2016.12.009.

Ambudkar IS. Ca^{2+} signaling and regulation of fluid secretion in salivary gland acinar cells. Cell Calcium. 2014 Jun;55(6):297-305. doi: 10.1016/j.ceca.2014.02.009.

Ambudkar IS. Calcium signalling in salivary gland physiology and dysfunction. J Physiol. 2016 Jun 1;594(11):2813-24. doi: 10.1113/JP271143.

Anderson GR, Aoto J, Tabuchi K, Foldy C, Covy J, Yee AX, Wu D, Lee SJ, Chen L, Malenka RC, Sudhof TC. Beta-neurexins control neural circuits by regulating synaptic endocannabinoid signaling. Cell. 2015 Jul 30;162(3):593-606.

Asraf H, Salomon S, Nevo A, Sekler I, Mayer D, Hershfinkel M. The ZnR/GPR39 interacts with the CaSR to enhance signaling in prostate and salivary epithelia. J Cell Physiol. 2014 Jul;229(7):868-77. doi: 10.1002/jcp.24514.

Baker OJ, Camden JM, Rome DE, Seye CI, Weisman GA. P2Y2 nucleotide receptor activation up-regulates vascular cell adhesion molecule-1 expression and enhances lymphocyte adherence to a human submandibular gland cell line. Mol Immunol. 2008 Jan;45(1):65-75.

Bemben MA, Nguyen QA, Wang T, Li Y, Nicoll RA, Roche KW. Autism-associated mutation inhibits protein kinase C-mediated neuroligin-4X enhancement of excitatory synapses. Proc Natl Acad Sci U S A. 2015 Feb 24;112(8):2551-6. doi: 10.1073/pnas.1500501112. Epub 2015 Feb 9

Charron F, Tessier-Lavigne M. Novel brain wiring functions for classical morphogens: a role as graded positional cues in axon guidance. Development. 2005 132(10):2251-62.

Cheng KT, Liu X, Ong HL, Ambudkar IS. Functional requirement for Orai1 in store-operated TRPC1-STIM1 channels. J Biol Chem. 2008 May 9;283(19):12935-40.

Choi SY, Lee K, Park Y, Lee SH, Jo SH, Chung S, Kim KT. Non-dioxin-like polychlorinated biphenyls inhibit G-protein coupled receptor-mediated Ca^{2+} signaling by blocking store-operated Ca^{2+} entry. PLoS One. 2016 Mar 10;11(3):e0150921.

Collins SJ, Ruscetti FW, Gallagher RE, Gallo RC. Terminal differentiation of human promyelocytic leukemia cells induced by dimethyl sulfoxide and other polar compounds. Proc Natl Acad Sci U S A. 1978 May;75(5):2458-62.

Damas J, Bourdon V. The release of glandular kallikrein from submaxillary glands of rats exposed to heat. Arch Int Physiol Biochim Biophys. 1994 May-Jun;102(3):183-8.

Décarie A, Raymond P, Gervais N, Couture R, Adam A. Serum interspecies differences in metabolic pathways of bradykinin and [des-Arg9]BK: influence of enalaprilat. Am J Physiol. 1996 Oct;271(4 Pt 2):H1340-7.

DeHaven WI, Jones BF, Petranka JG, Smyth JT, Tomita T, Bird GS, Putney JW Jr (2009) TRPC channels function independently of STIM1 and Orai1. J Physiol 587:2275-98.

Dijkhuizen T, van Essen T, van der Vlies P, Verheij JB, Sikkema-Raddatz B, van der Veen AY, Gerssen-Schoorl KB, Buys CH, Kok K (2006) FISH and array-CGH analysis of a complex chromosome 3 aberration suggests

that loss of CNTN4 and CRBN contributes to mental retardation in 3pter deletions. Am J Med Genet A 140:2482–2487.

Dörr K, Kilch T, Kappel S, Alansary D, Schwär G, Niemeyer BA, Peinelt C. Cell type-specific glycosylation of Orai1 modulates store-operated Ca^{2+} entry. Sci Signal. 2016 Mar 8;9(418):ra25. doi: 10.1126/scisignal.aaa9913.

Dragoni S, Laforenza U, Bonetti E, Reforgiato M, Poletto V, Lodola F, Bottino C, Guido D, Rappa A, Pareek S, Tomasello M, Guarrera MR, Cinelli MP, Aronica A, Guerra G, Barosi G, Tanzi F, Rosti V, Moccia F. Enhanced expression of Stim, Orai, and TRPC transcripts and proteins in endothelial progenitor cells isolated from patients with primary myelofibrosis. PLoS One. 2014 Mar 6;9(3):e91099.

Feske S. ORAI1 and STIM1 deficiency in human and mice: roles of store-operated Ca^{2+} entry in the immune system and beyond. Immunol Rev. 2009 Sep;231(1):189-209.

Genaro AM, Stranieri GM, Borda E. Involvement of the endogenous nitric oxide signalling system in bradykinin receptor activation in rat submandibular salivary gland. Arch Oral Biol. 2000 Sep;45(9):723-9.

Gillis S, Watson J. Biochemical and biological characterization of lymphocyte regulatory molecules. V. Identification of an interleukin 2-producing human leukemia T cell line. J Exp Med. 1980 Dec 1;152(6):1709-19.

Gobeil F, Filteau C, Pheng LH, Jukic D, Nguyen-Le XK, Regoli D. In vitro and in vivo characterization of bradykinin B2 receptors in the rabbit and the guinea pig. Can J Physiol Pharmacol. 1996 Feb;74(2):137-44.

Graham FL, Smiley J, Russell WC, Nairn R. Characteristics of a human cell line transformed by DNA from human adenovirus type 5. J Gen Virol. 1977 Jul;36(1):59-74.

Grynkiewicz G, Poenie M, Tsien RY. A new generation of Ca^{2+} indicators with greatly improved fluorescence properties. J Biol Chem. 1985 Mar 25;260(6):3440-50.

Gutiérrez-Venegas G1, Arreguín-Cano JA, Hernández-Bermúdez C. Bradykinin promotes Toll like receptor-4 expression in human gingival fibroblasts. Int Immunopharmacol. 2012 Dec;14(4):538-45.

Gwozdz T, Dutko-Gwozdz J, Schafer C, Bolotina VM. Overexpression of Orai1 and STIM1 proteins alters regulation of store-operated Ca^{2+} entry by endogenous mediators. J Biol Chem. 2012 Jun 29;287(27):22865-72.

Heo DK, Lim HM, Nam JH, Lee MG, Kim JY. Regulation of phagocytosis and cytokine secretion by store-operated calcium entry in primary isolated murine microglia. Cell Signal. 2015 Jan;27(1):177-86.

Hershfinkel M, Moran A, Grossman N, Sekler I. A zinc-sensing receptor triggers the release of intracellular Ca^{2+} and regulates ion transport. Proc Natl Acad Sci U S A. 2001 Sep 25;98(20):11749-54.

Hershfinkel M. The Zinc Sensing Receptor, ZnR/GPR39, in Health and Disease. Int J Mol Sci. 2018 Feb 1;19(2). pii: E439. doi: 10.3390/ijms19020439.

Heusch G, Bøtker HE, Przyklenk K, Redington A, Yellon D. Remote ischemic conditioning. J Am Coll Cardiol. 2015 Jan 20;65(2):177-95.

Higgins JJ, Hao J, Kosofsky BE, Rajadhyaksha AM (2008) Dysregulation of large-conductance Ca 2-activated K channel expression in nonsyndromal mental retardation due to a cereblon p.R419X mutation. Neurogenetics 9:219 –223.

Higgins JJ, Pucilowska J, Lombardi RQ, Rooney JP (2004) A mutation in a novel ATP-dependent lon protease gene in a kindred with mild mental retardation. Neurology 63:1927–1931.

Jin M, Hwang SM, Koo NY, Kim B, Kho HS, Choi SY, Song YW, Park K. Autoantibodies in Sjögren's syndrome patients acutely inhibit muscarinic receptor function. Oral Dis. 2012 Mar;18(2):132-9.

Kang JH, Kim DJ, Choi BK, Park JW. Inhibition of malodorous gas formation by oral bacteria with cetylpyridinium and zinc chloride. Arch Oral Biol. 2017 Dec;84:133-138. doi: 10.1016/j.archoralbio.2017.09.023.

Kaplan AP, Joseph K. Pathogenic mechanisms of bradykinin mediated diseases: dysregulation of an innate inflammatory pathway. Adv Immunol. 2014;121:41-89.

Kim JH, Park SH, Moon YW, Hwang S, Kim D, Jo SH, Oh SB, Kim JS, Jahng JW, Lee JH, Lee SJ, Choi SY, Park K. Histamine H1 receptor induces cytosolic calcium increase and aquaporin translocation in human salivary gland cells. J Pharmacol Exp Ther. 2009 Aug;330(2):403-12.

Kim N, Shin Y, Choi S, Namkoong E, Kim M, Lee J, Song Y, Park K. Effect of Antimuscarinic Autoantibodies in Primary Sjögren's Syndrome. J Dent Res. 2015 May;94(5):722-8. doi: 10.1177/0022034515577813.

Korkmaz Y, Bloch W, Steinritz D, Baumann MA, Addicks K, Schneider K, Raab WH. Bradykinin mediates phosphorylation of eNOS in odontoblasts. J Dent Res. 2006 Jun;85(6):536-41.

Landman N, Jeong SY, Shin SY, Voronov SV, Serban G, Kang MS, Park MK, Di Paolo G, Chung S, Kim TW. Presenilin mutations linked to familial Alzheimer's disease cause an imbalance in phosphatidylinositol 4,5-bisphosphate metabolism. Proc Natl Acad Sci U S A. 2006 Dec 19;103(51):19524-9.

Lee MG, Ohana E, Park HW, Yang D, Muallem S. Molecular mechanism of pancreatic and salivary gland fluid and HCO3 secretion. Physiol Rev. 2012 Jan;92(1):39-74. doi: 10.1152/physrev.00011.2011.

Leeb-Lundberg LM, Marceau F, Müller-Esterl W, Pettibone DJ, Zuraw BL. International union of pharmacology. XLV. Classification of the kinin receptor family: from molecular mechanisms to pathophysiological consequences. Pharmacol Rev. 2005 Mar;57(1):27-77.

Liu J, Ye J, Zou X, Xu Z, Feng Y, Zou X, Chen Z, Li Y, Cang Y (2014). CRL4A(CRBN) E3 ubiquitin ligase restricts BK channel activity and prevents epileptogenesis. Nat Commun. 21;5:3924. doi: 10.1038/ncomms4924.

Liu X, Gong B, de Souza LB, Ong HL, Subedi KP, Cheng KT, Swaim W, Zheng C, Mori Y, Ambudkar IS. Radiation inhibits salivary gland function by promoting STIM1 cleavage by caspase-3 and loss of SOCE through a TRPM2-dependent pathway. Sci Signal. 2017 Jun 6;10(482). pii: eaal4064. doi: 10.1126/scisignal.aal4064.

Lopez JJ, Albarran L, Gómez LJ, Smani T, Salido GM, Rosado JA. Molecular modulators of store-operated calcium entry. Biochim Biophys Acta. 2016 Aug;1863(8):2037-43.

Marceau F, Regoli D. Bradykinin receptor ligands: therapeutic perspectives. Nat Rev Drug Discov. 2004 Oct;3(10):845-52.

Martin AC, Willoughby D, Ciruela A, Ayling LJ, Pagano M, Wachten S, Tengholm A, Cooper DM. Capacitative Ca^{2+} entry via Orai1 and stromal interacting molecule 1 (STIM1) regulates adenylyl cyclase type 8. Mol Pharmacol. 2009 Apr;75(4):830-42.

Maurer M, Bader M, Bas M, Bossi F, Cicardi M, Cugno M, Howarth P, Kaplan A, Kojda G, Leeb-Lundberg F, Lötvall J, Magerl M. New topics

in bradykinin research. Allergy. 2011 Nov;66(11):1397-406. doi: 10.1111/j.1398-9995.2011.02686.x.

McElroy SP, Drummond RM, Gurney AM. Regulation of store-operated Ca^{2+} entry in pulmonary artery smooth muscle cells. Cell Calcium. 2009 Aug;46(2):99-106.

Melvin JE, Yule D, Shuttleworth T, Begenisich T. Regulation of fluid and electrolyte secretion in salivary gland acinar cells. Annu Rev Physiol. 2005;67:445-69. Review.

Mikoshiba K, Hisatsune C, Futatsugi A, Mizutani A, Nakamura T, Miyachi K. The role of Ca^{2+} signaling in cell function with special reference to exocrine secretion. Cornea. 2008 Sep;27 Suppl 1:S3-8. doi: 10.1097/ICO.0b013e31817f246e.

Missler M, Sudhof TC, Biederer T. Synaptic cell adhesion. Cold Spring Harb Perspect Biol. 2012 Apr 1;4(4):a005694

Nakao S, Ogata Y, Modéer T, Segawa M, Furuyama S, Sugiya H. Bradykinin induces a rapid cyclooxygenase-2 mRNA expression via Ca^{2+} mobilization in human gingival fibroblasts primed with interleukin-1 beta. Cell Calcium. 2001 Jun;29(6):446-52.

Namkoong E, Lee SW, Kim N, Choi Y, Park K. Effect of anti-muscarinic autoantibodies on leukocyte function in Sjögren's syndrome. Mol Immunol. 2017 Oct;90:136-142. doi: 10.1016/j.molimm.2017.07.007.

Oh HG, Chun YS, Kim Y, Youn SH, Shin S, Park MK, Kim TW, Chung S. Modulation of transient receptor potential melastatin related 7 channel by presenilins. Dev Neurobiol. 2012 Jun;72(6):865-77. doi: 10.1002/dneu.22001.

Palleschi S, Rossi B, Diana L, Silvestroni L. Di(2-ethylhexyl)phthalate stimulates Ca^{2+} entry, chemotaxis and ROS production in human granulocytes. Toxicol Lett. 2009 May 22;187(1):52-7.

Papuc SM, Hackmann K, Andrieux J, Vincent-Delorme C, Budis¸teanu M, Arghir A, Schrock E, T¸ut¸ulan-Cunit¸a˘ AC, Di Donato N (2015) Microduplications of 3p26.3p26.2 containing CRBN gene in patients with intellectual disability and behavior abnormalities. Eur J Med Genet 58: 319 –323.

Parekh AB. Store-operated CRAC channels: function in health and disease. Nat Rev Drug Discov. 2010 May;9(5):399-410.

Peralta FA, Huidobro-Toro JP. Zinc as Allosteric Ion Channel Modulator: Ionotropic Receptors as Metalloproteins. Int J Mol Sci. 2016 Jul 2;17(7). pii: E1059. doi: 10.3390/ijms17071059.

Proctor GB. The physiology of salivary secretion. Periodontol 2000. 2016 Feb;70(1):11-25. doi: 10.1111/prd.12116.

Rothwell PE, Fuccillo MV, Maxeiner S, Hayton SJ, Gokce O, Lim BK, Fowler SC, Malenka RC, Sudhof TC. Autism-associated neuroligin-3 mutations commonly impair striatal circuits to boost repetitive behaviors. Cell. 2014 Jul 3;158(1):198-212.

Roussa E. Channels and transporters in salivary glands. Cell Tissue Res. 2011 Feb;343(2):263-87. doi: 10.1007/s00441-010-1089-y.

Salmon MD, Ahluwalia J. Actions of calcium influx blockers in human neutrophils support a role for receptor-operated calcium entry. Cell Immunol. 2010;262(1):6-10.

Sawada Y, Kayakiri H, Abe Y, Mizutani T, Inamura N, Asano M, Aramori I, Hatori C, Oku T, Tanaka H. A new class of nonpeptide bradykinin B(2) receptor ligand, incorporating a 4-aminoquinoline framework.

Identification of a key pharmacophore to determine species difference and agonist/antagonist profile. J Med Chem. 2004 May 6;47(10):2667-77.

Schaff UY, Dixit N, Procyk E, Yamayoshi I, Tse T, Simon SI. Orai1 regulates intracellular calcium, arrest, and shape polarization during neutrophil recruitment in shear flow. Blood. 2010 Jan 21;115(3):657-666.

Sekler I, Sensi SL, Hershfinkel M, Silverman WF. Mechanism and regulation of cellular zinc transport. Mol Med. 2007 Jul-Aug;13(7-8):337-43.

Sekler I, Silverman WF. Zinc homeostasis and signaling in glia. Glia. 2012 May;60(6):843-50. doi: 10.1002/glia.22286.

Sensi SL, Paoletti P, Koh JY, Aizenman E, Bush AI, Hershfinkel M. The neurophysiology and pathology of brain zinc. J Neurosci. 2011 Nov 9;31(45):16076-85. doi: 10.1523/JNEUROSCI.3454-11.2011.

Seo J, Koo NY, Choi WY, Kang JA, Min JH, Jo SH, Lee SJ, Oh SB, Kim JS, Lee JH, Choi SY, Park K. Sphingosine-1-phosphate signaling in human submandibular cells. J Dent Res. 2010 Oct;89(10):1148-53. doi: 10.1177/0022034510376044.

Sharir H, Hershfinkel M. The extracellular zinc-sensing receptor mediates intercellular communication by inducing ATP release. Biochem Biophys Res Commun. 2005 Jul 8;332(3):845-52.

Sheereen A, Alaamery M, Bawazeer S, Al Yafee Y, Massadeh S, Eyaid W (2017) A missense mutation in the CRBN gene that segregates with intellectual disability and self-mutilating behaviour in a consanguineous saudi family. J Med Genet 54:236 –240.

Siddiqui TJ, Craig AM. Synaptic organizing complexes. Curr Opin Neurobiol. 2011 Feb;21(1):132-43.

Stojic D. Effects of captopril and bradykinin on chorda tympani-induced

salivation in cat. Eur J Oral Sci. 1999 Feb;107(1):21-4.

Suzuki N, Nakano Y, Watanabe T, Yoneda M, Hirofuji T, Hanioka T. Two mechanisms of oral malodor inhibition by zinc ions. J Appl Oral Sci. 2018 Jan 18;26:e20170161. doi: 10.1590/1678-7757-2017-0161.

Takahashi K, Yokota M, Ohta T. Molecular mechanism of 2-APB-induced Ca^{2+} influx in external acidification in PC12. Exp Cell Res. 2014 May 1;323(2):337-45.

Vallee BL, Falchuk KH. The biochemical basis of zinc physiology. Physiol Rev. 1993 Jan;73(1):79-118.

Vandenberghe M, Raphaël M, Lehen'kyi V, Gordienko D, Hastie R, Oddos T, Rao A, Hogan PG, Skryma R, Prevarskaya N. ORAI1 calcium channel orchestrates skin homeostasis. Proc Natl Acad Sci U S A. 2013 Dec 10;110(50):E4839-48.

Xu X, Ali S, Li Y, Yu H, Zhang M, Lu J, Xu T. 2-Aminoethoxydiphenyl Borate Potentiates CRAC Current by Directly Dilating the Pore of Open Orai1. Sci Rep. 2016 Jul 4;6:29304.

Yoo AS, Cheng I, Chung S, Grenfell TZ, Lee H, Pack-Chung E, Handler M, Shen J, Xia W, Tesco G, Saunders AJ, Ding K, Frosch MP, Tanzi RE, Kim TW. Presenilin-mediated modulation of capacitative calcium entry. Neuron. 2000 Sep;27(3):561-72.

Yule DI. Subtype-specific regulation of inositol 1,4,5-trisphosphate receptors: controlling calcium signals in time and space. J Gen Physiol. 2001 May;117(5):431-4.

Zou W, Meng X, Cai C, Zou M, Tang S, Chu X, Wang X, Zou F. Store-operated Ca^{2+} entry (SOCE) plays a role in the polarization of neutrophil-like HL-60 cells by regulating the activation of Akt, Src, and Rho family GTPases. Cell Physiol Biochem. 2012;30(1):221-37.

국문 초록

칼슘신호를 통한
말초 기관의 신경 조절 연구

김 윤 정

서울대학교 대학원

치의과학과 신경생물학 전공

시냅스는 두 신경세포가 신호를 주고받는 신경세포내의 기본 구조물로서 이를 중심으로 하는 많은 연구들이 신경세포의 세포간 신호전달 기능을 밝히고 있다. 시냅스의 구조와 기능조절에 대한 이해는 뇌기능 연구의 핵심이자 synaptopathy로 인한 뇌질환을 극복하는데 매우 중요하다. 신경세포는 외분비선과 근육 등을 포함한 우리 몸의 많은 장기들을 통제하는 역할을 수행한다. 중추신경뿐만 아니라 말초신경에서도 시냅스를 중심으로 한 신경세포와 다른 세포간의 신호전달은 매우 중요한 의의를 가지며, 이들에 대한 연구들은 해당 장기(organ)의 신경조절을 분자 및 세포차원에서 이해하는데 필수적이다.

말초신경계 중 하나인 타액선은 신경전달물질에 의한 세포 내 칼슘신호를 통해 그들의 분비 기능을 조절한다. 세포 내 Ca^{2+}의

증가는 세포 내 다양한 도메인에서 이온통로의 활성을 조절하고 AQP5 채널의 막 이동을 유도하여 물 분비를 일으킨다. 이러한 타액선 세포는 G-단백질 연결 수용체들 (GPCRs)을 통하여 다른 세포들과 신호를 전달한다. 따라서 외분비선을 포함한 여러 장기에서의 GPCR 을 이해하는 것은 신경으로부터 전달 되는 신호가 어떻게 수용되는지를 이해하는 데 매우 중요하다.

첫 번째로, 타액선에서 GPCR 신호 전달의 분자 메커니즘을 특성화했다. 최근 SOCE 는 GPCR 경유 Ca^{2+} 유입에 크게 기여함이 밝혀졌지만 아직까지 비흥분성세포에서 SOCE 특성을 비교한 연구는 잘 이루어져 있지 않다. 1 장에서는 인간 악하선 HSG 세포와 PC12 세포, HEK293 세포, Jurkat-T 세포 및 HL-60 세포의 SOCE 특성을 비교분석 하였다. 결과적으로, HSG 세포는 전형적인 Orai 의존 SOCE 를 갖는 대부분의 비흥분성 세포와는 구별된다는 것을 확인했다.

다음으로 타액선 세포에서 새로운 GPCR 을 밝혀 냈다. 2 장에서는 인간의 턱밑 샘 세포에서 대사성 Zn 수용체를 확인하고 그 특성을 분석하였다. 그 결과 ZnR / GPR39 가 인간 턱밑샘 세포에서 발현한다는 것을 발견했으며, Zn 는 cytosolic Ca^{2+} 농도 ($[Ca^{2+}]_i$)를 증가시켰다. 흥미롭게도, Zn 에 의한 $[Ca^{2+}]_i$ 증가가 muscarnic antagonist 와 histaminergic antagonist 에 의해 억제되지 않았으나, PLC inhibitor 에 의해서는 완전히 억제됨으로써 이종 탈 감작을 보였다. 이러한 결과들은 인간의 타액선세포에서 대사성 Zn^{2+} 수용체가 기존에 알려진 타액선

GPCR 과 구별되는 Ca^{2+} 신호 전달을 유도함으로써 타액분비를 조절함을 의미한다.

또한, 타액선 세포에서 GPCR 신호 전달 조절제를 연구했다. 3 장에서는 chlorpromazine 이 타액선의 세포내 칼슘 신호기전을 어떻게 조절하는지에 대한 연구 결과를 다뤘다. 생쥐 동물모델에서 chlorpromazine 은 무스카린 수용체 자극에 의한 타액분비를 억제하였다. Chlorpromazine 은 또한 인간의 타액선세포에서 무스카린 및 히스타민에 의한 세포 내 칼슘증가를 억제하였으며, 흥미롭게도 thapsigargin 에 의한 칼슘증가도 억제하였다. 이러한 결과는 chlorpromazine 이 ER 및 SOCE 와 같은 다양한 저해 부위를 통해 GPCR 매개 된 칼슘 신호를 억제함으로써 타액 분비를 감소 시킨다는 것을 시사한다.

마지막으로 근육 세포에서 GPCR 로 유도 된 Ca^{2+} 신호의 downstream 조절에 대해 연구했다. Ca^{2+} activated K$^+$ channel 인 BK channel 은 cytosolic Ca^{2+} 신호의 downstream 이다. 이 BK channel 의 세포막 표면 수준의 조절인자로 cereblon (CRBN)이 알려져 있다. 4 장에서는 pathogenic R419X 가 CRBN KO mutant 에서 관찰되는 phenotype 을 rescue 하는지 확인하고자 했다. *Drosophila* NMJ 를 이용하여 null mutant 에서 관찰되는 release probability 의 감소를 R419X 가 rescue 하지 못하는 것을 확인했으며, 또한 CRBN WT 이 brain 영역에서 발현되는 반면 CRBN R419X 는 VNC 및 axonal terminal 영역에서 발현됨을 확인함으로써, targeting defect 가 있음을 관찰했다. Cultured hippocampal neuron 영역에서도 CRBN KO cell 에 CRBN WT 를

transfection 하면 BK channel activity 가 감소하지만, CRBN R419X 를 transfection 시 BK channel 의 유의적인 감소를 보이지 않았다. 이러한 결과는 BK channel 증가를 통한 presynaptic release probability 의 감소가 CRBN KO 과 point mutation (R419X)에 의해 유도 될 수 있음을 시사한다.

이러한 결과들은 Ca^{2+} 신호에서 upstream (GPCR)과 downstream (Ca^{2+} − activated K^+ channel) 인자들이 말초 신경 전달에 대한 중요한 조절 인자로 작용하며, 외분비선과 근육을 포함한 말초신경 기능의 핵심적인 조절자 타겟이라는 것을 의미한다.